Palaeogeography, Palaeoclimatology, Palaeoecology
August 2021, Volume 576 Pages 110500 (21p.)
https://doi.org/10.1016/j.palaeo.2021.110500
https://archimer.ifremer.fr/doc/00697/80869/

Deglacial to Holocene environmental changes in the northern Ligurian Sea: The dual influence of regional climate variability and large-scale intermediate Mediterranean circulation

Le Houedec Sandrine [1, *], Mojtahid Meryem [1], Ciobanu Maria Cristina [2], Jorry Stephan [2], Bouhdayad Fatima Zohra [3], Guyonneau Emma [1], Sourice Stéphane [1], Toucanne Samuel [2]

[1] LPG-BIAF UMR-CNRS 6112, UNIV Angers, CNRS, 2 bd Lavoisier, 49045 Angers Cedex 01, France
[2] IFREMER, Unité de Recherche Géosciences Marines, Laboratoire Géodynamique et enregistrement Sédimentaire, CS10070, F-29280 Plouzané, France
[3] Institute of Geology and Mineralogy, Faculty of Mathematics and Natural Sciences, University of Cologne, Otto-Fischer-Straße 14, 50674 Cologne, Germany

* Corresponding author : Sandrine Le Houedec, email address : sandrine.lehouedec@unige.ch

meryem.mojtahid@univ-angers.fr ; maria.ciobanu@u-psud.fr ; stephan.jorry@ifremer.fr ; bouhdayad.fatima@uni-koeln.de ; eguyonneau@etud.univ-angers.fr ; Samuel.Toucanne@ifremer.fr

Abstract :

The sedimentary archives of the Mediterranean Sea record periodic deposits of organic-rich deposits, called sapropels in the eastern basin and organic-rich layers (ORL) in the western basin. Changes in both the Mediterranean circulation and inputs of fresh water through borderlands rivers under more humid climate, are important mechanisms to explain those events. The last ORL and sapropel S1 have different timing, respectively from ~14.5 to 9 Ka and from ~10 to 6 Ka, presumably due to different forcing factors in the western basin (i.e., melting of Alps ices). Here we present a high-resolution study of a marine sediment core located off the mouth of the Var River, one of the most dynamic river system of the northern borderland of the western Mediterranean Sea. We applied a multi-proxy approach based on benthic foraminiferal assemblages, foraminiferal δ18O and δ13C, grain size analyses, organic carbon content and XRF elemental data to decipher the regional climate signals from the basin-scale intermediate circulation signature. Our results do not show large river inputs at the timing of the last ORL deposit. On the opposite, foraminiferal and geochemical evidence indicate that the 11–6 kyr period, concomitant to Sapropel S1 event in the Eastern Mediterranean, was characterised by high river activity and low ventilated bottom waters at the studied location. Additionally, our results characterized the last 6 ka with large scale episodes of more active bottom water ventilation due perhaps to enhanced wind activity under an overall cooler climate.

Time series analyses were computed from stable isotopes, Ca/Ti XRF ratio and foraminifera abundances. They show common frequencies peaks (2.2–3, 1.1–1.2, 0.9–1.0, and 0.4–0.5 kyr) most likely related to the solar activity. Also, a specific frequency band (1.5–1.6 kyr) was only recorded in benthic foraminiferal

abundance and stable isotopic records. This was preferentially attributed to an oceanic-driven internal forcing.

Highlights

► Benthic foraminifera assemblages in the Western Mediterranean over the last 15 kyr ► Benthic environment response to past sub-orbital climate variability ► Impact of the Eastern Mediterranean LIW dynamic on the Ligurian bottom environment ► Active bottom water ventilation under Late Holocene cooler climate episodes

Keywords : Foraminifera, Paleoclimatology, Western Mediterranea, Holocene

1. Introduction

The Mediterranean Sea is a semi enclosed basin of relatively small size connected to the Atlantic Ocean through the Gibraltar Strait and located between temperate and tropical climatic zones. Those features make this region and the Mediterranean thermohaline circulation a complex system dually influenced by both European and North African climate. Strong climate-ocean interplay makes of the Mediterranean realm one of the most vulnerable region to climate change in Europe (e.g. Giorgi, 2006; Lionello et al., 2006; Turco et al., 2015). The most spectacular evidence of ocean-atmosphere connexion during the Neogene and the Quaternary are certainly the periodic deposits of organic-rich deposits, called sapropels in the eastern basin (e.g. Rossignol-Strick, 1985; Rohling et al., 1994; 2015) and organic-rich layers (ORL) in the western basin (e.g. Rogerson et al., 2008; Incarbona and Sprovieri, 2020; Pérez-Asensio et al., 2020). While eastern deposits might be found at sites as shallow at 300-400 m (Rohling et al., 1993, Murat, 1991), the western ORL are commonly found at deeper sites, below ~ 1500m (Cacho et al., 2002, Rogerson et al., 2008). In both cases, those organic rich deposits, are usually well laminated with elevated organic carbon content that typically range between 1 and 10% (Kidd et al., 1978). They are also characterized by markers of low bottom water oxygen conditions (e.g., in benthic foraminifera assemblage, e.g., Rohling et al., 1997; Jorissen, 1999; Mercone et al., 2001; Casford et al., 2003; Schmiedl et al., 2003; Kuhnt et al., 2007; Abu-Zied et al., 2008; Rogerson et al., 2008; Schmiedl et al., 2010, Le Houedec et al., 2020; Pérez-Asensio et al., 2020) and high surface productivity as suggested by high Ba concentration (e.g., Jimenez-Espejo et al., 2007; Meyers and Arnaboldi, 2005, Higgs et al., 1994; Thomson et al., 1995; Van Santvoort et al., 1996, 1997; De Lange et al., 2008).

The periodic formation of Eastern Mediterranean sapropels seems to be the result of astronomical forcing (Rohling & Hilgen, 1991; Lourens et al., 1996) which corresponds to phases of maximum of insolation enhancing monsoon activity and freshwater discharge from North African rivers (Rossignol-Strick et al., 1982, 1985; Rohling et al., 2002, 2015; Marino et al., 2009; Hennekam et al., 2014; Weldeab et al., 2014). Interactions between high productivity, terrestrial inputs and bottom environmental conditions favouring good preservation of the organic matter are the common explanation to explain the formation of sapropels (Casford et al., 2003; Rohling et al., 2015). Thus, modifications in the intermediate-deep water circulation are necessarily involved to promote sapropel deposition (Rogerson et al., 2008; Grimm et al., 2015; Rohling et al., 2015).

In the western Mediterranean Sea (WMed Sea), ORL were also associated to both enhanced productivity presumably related to increased continental runoff (Meyers and Arnaboldi, 2005), and reduced deep ventilation leading to low oxygen content and high preservation of organic matter at the sea bottom (Rogerson et al., 2008).

Most of ORL and sapropels are expected to be deposited at the same time, because the intermediate water masses formed in Levantine basin (LIW) convey eastern Mediterranean salinity reduction into the western Mediterranean (Murat, 1999) enhancing the water column stratification. However, notable exceptions occurred, especially for the most recent ORL (Cacho et al., 2002, Rogerson et al., 2008). For instance, the deposition of the last ORL took place ca. 14.5-9 ka, i.e. during the deglaciation and early Holocene (Cacho et al., 2002; Rogerson et al., 2008; Martinez-Ruiz et al., 2015) while the most recent Sapropel event S1, occurred later from ~10 to 6 ka (Emeis et al., 2000; Ariztegui et al., 2000; Rohling et al., 2015). It was suggested that while the development of the last sapropel in the eastern basin was essentially responding to the diminution of the formation rate of dense deep water under

high Nile river runoff, the western basin responds to more complex forcing factors. In addition to injection of dense deep water, the Bernoulli aspiration through the Gibraltar strait, by modulating the rate of deep-water removal in the western basin, would be a second important factor to consider (Rohling et al., 2015). Those authors suggest that this process lower the chance of development of deep anoxia in the western basin. In the case of the last ORL deposit, the superimposed effect of alpine ices melting would have shallowed the depth of action of the Bernoulli effect, favouring deep anoxia as soon as 14.5 ka, explaining the asynchronous deposit between the last ORL and sapropel S1 (Rohling et al., 2015).

Since a few decades, it becomes clear that the North Atlantic climate influence is of great importance in the western basin hydrology (e.g. Rohling & Hilgen, 1991; Bard et al., 2002; Toucanne et al., 2015; Wagner et al., 2019). For instance, Italian terrestrial climatic archives (speleothems and lakes) support evidence of enhanced hydrological activity at the time of S1 (Zanchetta et al., 2007; Ariztegui et al., 2000; Magny et al., 2013). An enhanced hydrological activity was also demonstrated in the Gulf of Lion (Pasquier et al., 2019) and the Tyrrhenian sea for oldest organic-rich depositional events to which systematic decrease in salinity and intermediate circulation were observed (Kallel et al., 2000, Toucanne et al., 2012, 2015; Dixit et al., 2020). From those studies, it become evident that freshwater runoff in the western Mediterranean and particularly from its northern borderland has to be considered to understand the dynamic of the deposit of ORL. However, despite some terrestrial evidence of enhanced precipitation at the time of S1 in the north western Mediterranean, we lack of data to fully linked this oceanic event to enhanced river discharge in the area.

In this paper, we will focus on one of the most dynamic river system of the northern borderland of the western Mediterranean Sea, the Var river system. This river system, connected to the Alpine Ice Sheet during the last glacial period, is composed of several major

tributaries (i.e., Tinée, Vésubie, Var) draining the Alps. Today, the hydrological changes of the northern borderlands of western Mediterranean basin were shown to be dependent on the North Atlantic atmospheric circulation (Trigo et al., 2002; Kandiano et al., 2014). Thus, due to its very north location in the western Mediterranean, the Var river system is expected to be influenced also at millennial scale by the hydroclimatic variability of North Atlantic. We selected the marine sediment core KESC9–14 (537 m water depth) located off the mouth of the Var river (Figure 1) in the Ligurian sub-basin (WM Sea). The very proximity of the core to the Var river mouth makes it suitable to capture short-term regional environmental/climate variability. In addition, the Ligurian Sea is on the pathway of the Levantine Intermediate Water (LIW) originated from the Eastern Mediterranean (Millot, 1987, 1999, 2009). As such, core KESC9-14 has the advantage to retain both continental climatic influence through the river activity and marine environmental signals at high resolution (e.g. Jallali et al., 2018).

Here, we will focus on the last 15 kyr, covering the climatic variability of the last deglaciation and the time period of the deposit of the last ORL/sapropel event We present a multi proxy approach, combining benthic foraminiferal assemblages with foraminiferal oxygen and carbon stable isotopes, sedimentological (grain size) and geochemical analyses (XRF elemental data), in order to decipher the regional climate signals triggered by the activity of the French Riviera river system, from the basin-scale signature linked to intermediate water masses circulation in the Mediterranean.

2. Study area

2.1. The Var hydro-sedimentary system

The Ligurian Sea is fed by small rivers from the Southern French Alps and western Apennines. The Var River is the main water stream discharging sediments into the area and is

characterized by pronounced seasonal water discharge during autumn, season of heavy rainfall, and spring, season of snow melt (Sage, 1976; Xoplaki et al., 2004). Mean annual fluvial discharge is 70 m^3/s and can range from 20 m^3/s to over 800 m^3/s in a few hours (Dubar and Anthony, 1995). The Var drainage system (2800 km^2) extends from the southern French Alps to the Ligurian Sea (northwestern Mediterranean Sea). The drainage area is composed mainly of marls (e.g. Permian clays and silts, Callovo-Oxfordian black shales, and Jurassic and Cretaceous marls) (Kerckhove et al., 1980; Mulder et al., 1997).

The coast line in the area is characterized by a steep high-relief (from 6 to 11%) and a very narrow continental shelf (Piper and Savoye, 1993) leading to water depths of 2000 m at a distance of less than 20 km from the coast (Pautot, 1981; Figure 1). This results in a straight forwards connection between the Var river mouth and the deep Ligurian basin through submarine canyons during both high and low sea-level conditions (Pautot, 1981; Savoye et al., 1993; Migeon et al., 2006). This makes the Var sediment-routing system able to transmit climate-driven changes in sediment flux to the ocean (Bonneau et al., 2014). The very short connection between the Var River and the submarine canyon together with a high sediment discharge (~1.32-1.63 million tons/yr, (Mulder et al., 1997) explains the high sedimentation rate at the deep depositional system during the Holocene (Piper and Savoye, 1993, Mas et al., 2010). At the site, the sedimentation rate varied from 20 to 180 cm/Kyrs over the last 15 Ka (Figure 2)

2.2. Oceanographic settings

The surface current (the upper 100 to 200 m of the water column) of the Ligurian Sea, called the Northern Current (NC), flows westwards along the West Italian-south French coastline and transports the northern branch of the Modified Atlantic water (MAW, Millot,

1990, Millot and Taupier-Letage, 2005). The westward NC flow is the main hydrological feature of the Ligurian Sea as it is responsible for the redistribution of sediments delivered by rivers along the continental shelf (Bassetti et al., 2016). Below the inflowing surface MAW, from 200 down to 600 m-1000 m water depth, the Levantine Intermediate Water (LIW) is a westward flow originating from the eastern Mediterranean (Millot, 1987, 1999, 2009). The LIW is mainly formed during cool winters (Astraldi and Gasparini, 1992; Sparnocchia et al., 1995, 2013) and constitutes a significant part of the intermediate waters in the western Mediterranean basin (Millot and Taupier-Letage, 2005). Under strong north westerly winds cooling surface waters, an additional intermediate water mass is formed in the northwestern Mediterranean Sea, the Winter intermediate water, WIW (Salat and Font, 1987; Petrenko, 2003; Juza et al., 2013, 2019), also called Riviera Winter Water in the Ligurian Sea (Lacombe and Tchernia, 1960; Gasparini et al., 1999). The WIW is located at intermediate depths around 300-100 m, below AW and above LIW (Millot, 1999; Pinot and Ganachaud, 1999; Juza et al., 2019). Below ~1000 m depth, the Western Mediterranean Deep Water (WMDW) is present (Millot and Taupier-Letage, 2005). Here, because the studied core is today located at 537 m depth, it is bathed by the LIW and influenced seasonally by the WIW. However, over the last 15 kyr, a period characterized by a sea-level change and a strong climatic variability, the dynamics of these water masses might have been strongly affected.

The Ligurian Sea is also characterized by the common occurrence of coastal anticyclonic eddies, mainly during autumn and winter (e.g. Santoleri et al., 1983, Marullo et al., 1985). The intense vertical velocities of theses eddies induce strong, long-lasting coastal upwellings (Casella et al., 2011). These hydrological processes can generate bursts of nutrients into the euphotic layer with potentially important effects on primary production (Casella et al., 2011).

3. Material and methods

3.1. Age model

KESC9–14 core (43.31°N, 7.11°E; 537 m, Figure 1) was collected during the Ifremer ESSCAR-9 cruise in 2008 (Woerther, 2008). The age model of this core (Figure 2) is based on 14 AMS ^{14}C dates (Table 1) performed on planktonic foraminifera tests of different species and provided by the Beta Analytic Radiocarbon Dating Laboratory (Florida, USA) and the Poznan Radiocarbon Laboratory (Poland). The raw ^{14}C AMS radiocarbon dates were calibrated using R software (Bchron package; R Core Team, 2013) using the marine calibration curve IntCal~~13~~20 (Reimer et al., 2020) after applying a local reservoir age correction (400 ± 50 yr) obtained from the Global Marine Reservoir Database using the average of the ten nearest reservoir ages (http://calib.org/marine/).

3.2. Grain size and organic carbon analyses

Grain-size analyses of core KESC9-14 were performed on 50 decarbonated sediment samples with a Beckman Coulter LS200 laser diffraction particle size analyser at Ifremer (France). Grain size parameters (volumetric percentage of sand, silt and clay; the 50th percentile-D50-median grain size; the 90th percentile-D90) were calculated using GRADISTAT v 8.0 program (Blott and Pye, 2001), and grain size distribution spectra were computed (Figure 3). Before measurement, the sediment was oven-dried (36 H) at 35°C and treated with 3 ml of 1M HCl. Subsequently, the samples were centrifuged for 3min, washed twice with 6ml of distilled water and then analyzed.

The Total organic carbon (TOC) content was analyzed by combustion in a LECO CS 125 carbon analyzer (internal standard error ≤ 5 %) at Ifremer (France) following the protocol described by Ciobanu et al. (2012). Prior to analyses, the sediment samples (~ 0.3

g) were oven-dried (65°C) for 20 h, grounded in a mortar, then the inorganic carbon was removed by progressive and controlled acidification with diluted HCl as described in Cauwet (1981).

3.3. X-ray fluorescence (XRF) analysis

The X-ray fluorescence scanning of chemical elements (Ca, Si, Ti, Br, Cl, Mn, Al) was performed using an AVAATECH XRF core scanner (Rhodium, Rh, source) with an elemental standard deviation ≤ 3% at Ifremer (France). The entire length of the core was scanned with a 1 cm resolution with a count time of 20 s, by setting the voltage to 10 kV (no filter) and 30 kV (Pd thick filter) and the intensity to 200 µA and 1000 µA, respectively.

Because XRF core scanner instrumental performance may significantly be influenced by small matrix effects (Richter et al., 2006; Tjallingii et al., 2007), the raw total counts of each element were normalized to the total counts of all measured elements, excluding Rh (the XRF core scanner source), for the position (Bahr et al., 2014). To allow more robust statistical analyses, XRF ratios were converted to log-ratios (Tjallingii et al., 2007; Weltje and Tjallingii, 2008). We focus, in the present study, on the Ca/Ti ratio which is the common indicator of marine biogenic carbonate versus terrestrial input (Richter et al., 2006; Goudeau et al., 2014; Azuara et al., 2020).

In order to quantify some of the scanned elements (Ti, Si, Ca), 20 sediment samples were extracted and analyzed using Wavelength Dispersive X-Ray Fluorescence spectrometry (WD-XRF, Brucker S8, Ifremer, France). Prior to analyses, “glass” pellets were prepared after grounding and mixing sediments samples and transforming them into glass by fusion in an oven at ~1000 °C (El Maghraoui et al., 1999; Ciobanu et al., 2012). We obtained therefore percentages of TiO_2, SiO_2 and CaO.

3.4. Isotopic analyses

Stable oxygen ($\delta^{18}O$) and carbon ($\delta^{13}C$) isotopes were measured from 5-10 tests of the benthic species *Cibicidoides pachyderma* in 85 samples (~10 cm resolution) and from 15 tests of the planktic species *Globigerina bulloides* in 159 samples (~5 cm resolution). Both species were handpicked from the 250-300 μm fraction. The $\delta^{13}C$ and $\delta^{18}O$ were measured with a Finnigan MAT-253 mass spectrometer coupled to a Kiel-IV carbonate preparation device at Pôle Spectrométrie Océan (CNRS-UBO-Ifremer, Brest) with a standard deviation of 1.95±0.03 ‰ for $\delta^{13}C$ and -2.20±0.06 ‰ for $\delta^{18}O$ obtained from the NBS-19 standard. The $\delta^{18}O$ and $\delta^{13}C$ isotope measurements are reported in per mil (‰) relative to the Vienna PeeDee belemnite (VPDB).

In near-river marine settings, the interpretations of foraminiferal oxygen and carbon stable isotopes might be affected by various factors. While the benthic and planktic foraminiferal $\delta^{18}O$ reflect changes in temperatures and/or salinity, the $\delta^{13}C$ might be more complex. For planktic foraminifera, the $\delta^{13}C$ might reflect: (i) the surface productivity, because high photosynthetic activity leads to a depletion of ^{12}C in surface water and subsequently to higher $\delta^{13}C$ of planktic foraminifera, and/or (ii) the introduction of continental isotopically light DIC to surface waters with fluvial input inducing a decrease in the planktic $\delta^{13}C$ signature (e.g. Casford et al., 2002; Mojtahid et al., 2015). For benthic foraminiferal, the remineralization of ^{12}C-enriched phytodetritus induces a decrease in the benthic $\delta^{13}C$ values. However, an active bottom water ventilation with relatively high $\delta^{13}C$-DIC signature (compared to aged waters with low $\delta^{13}C$-DIC) will increase benthic $\delta^{13}C$ signature.

3.5. Foraminiferal benthic abundance

Benthic foraminiferal fauna was analysed in 88 subsamples with a 6 cm-resolution in average corresponding to ~60 yr (in the Late Holocene) – 100 yr (during the Late Pleistocene). Subsamples were washed through a 125 µm sieve and the small sized adult species that may compose a large part of the foraminiferal assemblage in the <125 µm fraction was not considered in this study. We however explored some samples from the 63-125 µm fraction and mostly juveniles of foraminifera from the large fraction are present. Because of the high foraminiferal abundances in some levels, samples were splitted into subsamples (aliquots) using an Otto Microsplitter. More than 200 specimens were picked from a single aliquot using a binocular microscope, stored in separate Chapman slides, and identified at a species level. The species relative abundances (%) were calculated and here we present only the dominant species with a relative abundance ≥5% in at least one sample (i.e. 21 species over the 174 species identified). See Data Availability section to access to the online complete raw data set. In order to help with taxonomical identification, Scanning Electron Microscope (SEM) photographs were obtained at SCIAM microscopy platform (Angers University, France) using the Zeiss EVO LS10 (Figure 7).

A principal component analysis (PCA) on covariance based on the relative abundances of the 21 major benthic species (≥5%) and the diversity index (Shannon H performed using the abundance of the 174 species) was computed using PAST software package PAleontological STatistics; Version 3.25; Hammer et al., 2001). To analyse the variation in the relative abundance record of the species over the last 15 kyr we calculated the normalized deviation to the mean in percent for each record.

3.6. Analysis of the embedded cyclicity

To shed light on the frequency embedded in the relative abundance spectrum as well as in geochemical records, REDFIT and Continuous Wavelet Transform (CWT, Morlet wavelet) analyses were processed using PAST software. The CWT were done on (benthic and planktic $\delta^{18}O$ and $\delta^{13}C$, Ln(Ca/Ti) and Ln(Br/Cl)) using pre-treated data as follows: (i) the records were linearly interpolated at even spaced time-resolution with a 25 years step for XRF ratios and respectively with a 93 and 185 years step for the planktic and benthic stable isotope's records. To highlight the cyclicity embedded in the foraminiferal relative abundances of the 21 dominant species, we used a REDFIT analysis. The 21 resulting spectra were compiled an average Redfit periodogram curve was computed. Prior to the CWT and REDFIT analyse, all data were detrended from the glacial/interglacial cycle using a bandpass filter (0.04-0.5).

4. Results

4.1. Age model and sedimentation rate

According to our age model, Core KESC9–14 covers a time period from 15.4 to 0.6 ka with a continuous sedimentation (i.e. without time inversions, Figure 2). Calculated sedimentation rates are on average 69 ± 50 cm ka^{-1} ranging from a minimum of 18 cm ka^{-1} (~10.4 – 8 ka) to maximum values of 171 $cm.ka^{-1}$ (~1.3 – 0.6 ka, Figure 2).

The sampling resolution for ^{14}C dating is high enough to provide good confidence in the calculated age model. An exception can be made however for the period from 15 to 11 ka encompassing the well-known B/A and YD periods which are well expressed in the planktic oxygen isotopic signature in most marine records from the Western Mediterranean (e.g. Cacho et al., 2001, 2002; Frigola et al., 2007, Toucanne et al., 2012). Because the age model is not very well constrained for this time period, the planktic $\delta^{18}O$ peak in our record marking the paroxysmal cold phase of the YD period is about 400 yr older than the well-known age of

~ 12.9–11.7 ka as defined from Greenland GISP2 ice-core (Alley et al., 1993; Meese et al., 1997). As such, in the few paragraphs discussing this time period, we will refer to the planktic $\delta^{18}O$ signature for the timing of the transition between the B/A and YD.

4.2. Lithological features and grain-size analyses

The visual description of Core KESC9–14 indicates the presence of rather homogeneous light grey (10YR 7/1/2 on Munsell color code: Munsell, 1912) silts apart from the bottom 15 cm of the core showing the presence of light grey coarse silts - fine sands (cf. core images Figure S1). Grain size analyses confirm this description with overall silty sediments presenting slightly higher proportions of sands prior to ~12.5 ka and increasing proportions of clays after ~6 ka (Figure 3). The grain size distribution shows a predominant 6-10 µm mode, except between 10.4 and 6.8 ka with a mode at 17-20 µm due to increasing proportions of medium to coarse silt (60-65%). Since ~5 ka, a second mode at around 105-110 µm is present in some samples that are mostly characterised by slightly coarser sediments (Figure 3).

D50 and D90 parameters generally show a similar pattern along the core, apart from the 11-6 kyr time interval (Figure 3). High values are recorded before ~13 ka, whereas overall low values are found from ~13 to 11 ka and after ~4.5 ka. During the 11-6 kyr time interval, D50 shows a rapid increase to reach maximal values from ~9.5 to 7 ka, followed a progressive decrease from ~7 to 4.5 ka. Meanwhile, the D90 remains generally constant at low to intermediate values. Since ~4.5 ka, both parameters show short term variations oscillating between periods of relatively high and low values (Figure 3).

4.3. Sediment geochemistry (WD-XRF, XRF and TOC data)

All the sediment geochemistry results are presented in Figure 3. The SiO_2 and TiO_2 (%) records show overall low values prior to ~12 ka (~45 and 0.56% respectively) with a slight peak at 13 ka. This was followed by a progressive decrease to reach high values (~50% and 0.64% respectively) at 6 ka. Over the last 6 kyr, the SiO_2 and TiO_2 percentages slightly decrease until ~2.5 ka, increase until ~1 ka before to decrease again at the end of the record. The opposite trend is shown by the CaO (%) record with values ranging from ~22 to 33 %.

The Ln(Ca/Ti) ratio record is very similar to the CaO(%) record, although with a much higher time resolution. Throughout the record, the TOC content varies from 0.37 to 0.66%. High values of TOC are found before ~13 ka, followed by a 0.2 %-decrease from 13 to 12.3 ka and then an increase until 6 ka. The TOC reaches its maximum values between 7.3 and 6 ka. From 6 to 3.8 ka, the TOC rapidly decreases, then strongly oscillates between 0.45 and 0.6 % over the last 4 kyr with high values centred at 2.9, 2.3 and 1.4 ka.

4.3. Foraminiferal stable isotopes

The carbon and oxygen stable isotopic records from benthic (*C. pachyderma*) and planktic (*G. bulloides*) foraminifers are plotted in Figure 4. The benthic $\delta^{13}C$ record describes three main phases: (i) from 15 to 10.5 ka the signature is highly irregular and oscillates around an average value of 0.8±0.6‰. (ii) From ~10 to 5 ka the benthic $\delta^{13}C$ values are low in average (0.5±0.3‰) and show two time intervals of low values (~10 to 8.5 ka and ~7.5 to 6 ka) interrupted by a brief period recording high $\delta^{13}C$ values (~0.9 ‰). (iii) Since 5 ka the record increases again to reach an average value of ~0.8±0.1‰ around which the record oscillates with 4 marked episodes of higher values at around 4.5, 3.5, 2.6 and 1.3 ka. The planktic $\delta^{13}C$ record shows an overall decreasing trend by around 1‰ from 12.5 to 6.5 ka.

Over the Late Holocene, the planktic $\delta^{13}C$ becomes highly variable with variations up to 1.5-2‰.

The benthic and planktic $\delta^{18}O$ records follow a general decreasing trend to low value (by around 2‰) from 15 to 10.5 ka. Then from 10.5 to 6.5 ka, and while the benthic record is relatively stable at around 1.5‰, the planktic record continues its decrease to reach a minimum of 0.7‰ between 9 and 6.5 ka. At 6.5 ka the planktic $\delta^{18}O$ record rises again by +0.5‰ and strongly oscillates since the last 6 kyr by ±0.5‰ with higher $\delta^{18}O$ values recorded at ~5.8, 4.5, 3.2 and 1.4 ka.

4.4. Benthic foraminiferal assemblages

A total number of 174 benthic foraminiteral species were determined along Core KESC9-14 (see Data Availability section in online supplemental material), among which 21 species are dominant (i.e. showing relative abundances ≥5% in at least one sample, Figures 5 and 6).

In order to facilitate examination of the large dataset obtained for Core KESC9-14 and to extract the main faunal ecological groups, a PCA analysis (axis 1 = 23% and axis 2 = 13%; Figure 5a) and a statistical analysis of the variability were performed on the relative abundance records of the 21 dominant species (Figure 5b). These statistical analyses separate the faunal assemblages into four species groups, each with a specific trend that can be described with an average spectrum (Figure 5c).

Group 1 (in green, Figures 5 and 6) is characterized by species showing high relative abundances from ~15 to 11 ka. *Uvigerina mediterranea*, *Bolivina spathulata* are the two most dominant species of Group 1 reaching respectively 35% and 25%, on average, of the total assemblage for this time period. These species show prominent peaks around 12 ka explaining

the minimum values of Shannon *H* index at the time (Figure 5c). While *B. spathulata* nearly disappears after 11 ka, *U. mediterranea* shows a progressive decrease until ~8.5 ka, to re-increase again until the core top (Figure 6). This group is also composed of minor contributors: *Textularia agglutinans* (up tp 9%), *Gyroidina soldanii* (up to 8%), and *Gyroidina orbicularis* (up to 6%).

Group 2 (in red, Figures 5 and 6) is characterized by species with high relative abundances between ~10 and 6-5.5 ka. This group is composed mainly of *Hyalinea balthica*, (9% on average during this time period), *Bulimina inflate* (~8%), *Globocassidulina subglobosa* (~5%) and only subsidiary of *Amphicoryna scalaris* (3%) and *Sphaeroidina bulloides* (2%). During the early Holocene, *H. balthica* increases in relative abundances to reach maximum values (~17%) at 8.4 ka, after which it decreases to reach about 5% in the late Holocene. *Bulimina inflata* follows a similar trend although the peak is reached later around 7.8 ka and a clear increase is recorded after ~1.8 ka. *Globocassidulina subglobosa* is nearly absent outside the 10 - 5.5 ka time interval.

Group 3 (in orange, Figures 5 and 6) clusters species with the highest abundances over the last ~6-5.5 ka. This group is highly dominated by *Melonis barleeanus* (17% on average during this time period), *Cibicidoides pachyderma* (8%) and *Valvulineria bradyana* (6%) and contains few specimens of *Cassidulina carinata* (5%), *Bolivina alata* (3%) and *Sigmoilopsis schlumbergeri* (2%). *Melonis barleeanus* shows a large variability and is also dominant between ~10 and 8 ka where it shows a pattern similar to *H. balthica*'s Group 2. After 6-5.5 ka, the percentages of *M. barleeanus* increased significantly from ~5 to 25 % around 5-3 ka, then decreased to reach ~15 % at ~2.7 ka. Another peak of ~27 % is recorded around ~1.7 ka, after which the percentages of this species decrease drastically to reach ~7% at the core top. Relative abundances of *C. pachyderma*, *V. bradyana* and *C. carinata* show a progressive

increase since 10-8 ka and a rather stable evolution after 6 ka. Although *C. carinata* clusters in Group 3, it is a dominant species during Termination 1.

Group 4 (in black, Figures 5 and 6) is not associated to a specific time period and is composed mainly of *Uvigerina peregrina* (8% on average along the entire record), *Pseudoclavulina crustata* (2 %) and *Bulimina marginata* (2%), *Globocassidulina crassa* (1%), *Adelosina* sp. (1%). These species are present through the sedimentary record with a relatively low variation and no specific pattern.

5. Discussion

On the basis of sedimentological, geochemical and foraminiferal analyses, our data highlight three time periods characterized by specific hydrological and climatological patterns: (i) the 15-11 kyr time interval being part of Termination I, (ii) the 11-6 kyr time interval concomitant to the deposition of the sapropel S1 in the deep eastern Mediterranean and (iii) the last 6 kyr, from mid- to late Holocene.

5.1. Ecological and hydrological changes of benthic environments in the Ligurian Sea across Termination I (before ~11 ka):

In the studied core, the period from ~15 to 11 ka is characterized by significant shifts in planktic $\delta^{18}O$ values that can be related to both major B/A and YD climatic events (Figure 4).

5.1.1 The Bølling–Allerød event

From the studied core, the overall lower planktic B/A-$\delta^{18}O$ values compared to the YD-$\delta^{18}O$ values (by ~0.5 ‰) might indicate warmer sea surface waters in the Ligurian Sea, and/or reflect higher input of fluvial freshwaters due to increased precipitation on the continent during the B/A period. This is coherent with the regional climatic studies describing generally the B/A as a warm and humid interstadial in opposite to the cold and dry climate for the YD (e.g. Pèrez-Obiol and Julià, 1994; Cacho et al., 1999, 2001; Combourieu Nebout et al., 1999, 2009; Allen et al., 2000; Allen and Huntley 2009; Naughton et al., 2007; Fletcher and Sánchez Goñi, 2008; Kotthoff et al., 2008a, b). However, although our planktonic foraminiferal $\delta^{18}C$ surface waters might reflect high fresh water influence during the B/A, the sedimentological proxies rather point to low fluvial activity (Figure 3). The decreasing trend of Ca/Ti ratio used here as an indicator of marine biogenic carbonate versus terrestrial input seems to indicate either a rather high oceanic primary productivity or a weakening of the fluvial activity over the B/A period, at least when compared to the Holocene period (Figure 3). Low river inputs are also supported by the relatively low TiO_2 and SiO_2 contents and low TOC values. It is consistent with the fact that the alpine ice, drained by the Var river system during the last glacial period, have melted before the B/A as previously shown by Bonneau et al. (2014; 2017). However, the contribution of southern French rivers through the melting of alps ice at that time was suggested as an important factor to explain the timing of the deposit of the last ORL (Rogerson et al., 2008; Rohling et al., 2015). From our data, the Var river system does not seem actively contribute to the alpine melt-water input during B/A. Therefore, the alpine melt water pulse might be rather provided by the Rhône River that drained more northern alpine ices that might be still stand at that time.

Despite the relatively low terrigenous inputs during the B/A, a high abundance of eutrophic and mostly opportunistic foraminiferal benthic species (Figure 6) such as *C. carinata/laevigata* as well as *U. mediterranea* and *B. spathulata* is observed (e.g., Jorissen et

al., 1992, De Rijk et al., 2000; Schmiedl et al., 2000; Fontanier et al., 2003; Goineau et al., 2011). This foraminiferal feature and the relatively low benthic $\delta^{13}C$ signature at that time seems to indicate an increase of the carbon export to the sea floor. A still active river activity during the B/A through precipitation (Combourieu-Nebout et al., 1998; Kotthoff et al., 2008a, b) while keeping a mild bottom circulation might explain this apparent paradox.

5.1.2 The Younger Dryas event

Contrary to the B/A, the YD period, especially in its beginning, is characterized in our sedimentological record by relative coarser sediment. Both D50 and D90 values are high, a bimodal grain size distribution is still recorded until ~13 Ka and a higher proportion of coarser sediment is recorded at the entrance of YD (Figure 3). In addition, the YD is characterised by relatively high benthic $\delta^{13}C$ values (Figure 4). Those sedimentological and geochemical features agreed to a reinforcement of bottom water circulation over this time period. An active bottom circulation will also prevent the accumulation of organic matter explaining the large decreasing trend observed in the TOC record over this time (Figure 3).

Studies tackling the general circulation of the western Mediterranean during the YD report a complex configuration between the deep and intermediate water depths. In the nearby Corsica Trough (McCulloch et al., 2010; Toucanne et al., 2012, Angue Minto'o et al., 2016), YD corresponds to an episode of more active intermediate circulation (i.e. active LIW at 500 m). At the contrary, in the deep Alboran sea (3000 m depth), this time period was still associated to the last ORL event, with enhanced surface primary productivity and a sluggish deep water circulation (Rogerson et al., 2008). Additionally, and because an overall dry climate characterized the YD over the adjacent continent (e.g. Pèrez-Obiol and Ramon, 1994;

Allen et al., 1996; Magny and Bégeot, 2004; Zanchetta et al., 2007; Regattierri et al., 2014), the winds were reported to be more active in WM (e.g. Cacho et al., 2001; Rodrigo-Gámiz et al., 2011).

Despite evidence of reduced OM content in the benthic environment, the dominance of the high organic flux species *U. mediterranea* and *B. spathulata* (De Rijk et al., 2000; Minto'o et al., 2016) indicates that eutrophic conditions still prevailed during the YD. On the other hand, *C. carinata/laevigata*, largely decreased over the YD (Figure 6), probably as a result of: i) the progressive deepening of the water column placing the studied core in an area which is no longer optimal for its growth, and/or ii) the decrease of downslope transport, to which this species is very often subject due to its flat-shaped test (e.g. Garcia et al., 2013; Mojtahid et al., 2013). The input of nutrients in the area through an active nutrient-rich intermediate circulation and/or an intense mixing of waters under the action of the winds will allow to maintain still eutrophic bottom environment. Therefore, we assume that the combination between an active nutrient-rich LIW passing through our study site and active winds mixing the water column might have maintained a rather eutrophic benthic environment as indicated by foraminifera.

5.2. Transition from early to the mid- Holocene (11 to 6 ka): evidence of organic-rich/low-oxygen time interval in the Ligurian Sea

From early to mid-Holocene, sediments of core KESC9-14 are significantly coarser than during the YD and the late Holocene (Figure 3). Contrary to the B/A period, the high values of D50 are not accompanied by high D90 values (due to high proportions of fine sands/coarse silts), but are due to higher proportions of medium to fine silts (Figure 3). These latter might have been brought to the study site in suspension in a period of enhanced river

runoff. This high fluvial influence is corroborated by the regularly decreasing Ca/Ti ratio that most likely indicates higher contribution of terrigenous particles as the core content become enriched in TiO_2 and SiO_2 during that time (Figure 3). By following the same decreasing trend as Ca/Ti, the progressively lower values of planktic $\delta^{13}C$ most likely reflect the influence of isotopically light DIC originating from continental river waters (Figure 4). In the same logic, we assume that the depleted planktic $\delta^{18}O$ values characterizing this time period, the lowest of the complete record ca. 9.5-8 ka, probably indicate the presence of fluvial freshwaters, (Figure 4). This is supported by the reconstruction of sea surface temperature from the nearby Gulf of Lion (Jalali et al., 2016, Figure 8) indicating rather stable temperature while our $\delta^{18}O$ significantly increases by around 0.5‰ between 9.5 - 8 ka. Our results are also coherent with the large $\delta^{18}O$ shift reported from the North Italian speleothem record from Corchia cave (Zanchetta et al., 2007) and interpreted as a period of enhanced precipitation on the continent (Figure 8). In fact, it is well-established that around 10-9 ka, during the Holocene maximum insolation, the rivers around Mediterranean Sea records a maximum flooding. This is well recorded in the eastern basin with the Nile River (Weldeab et al., 2014) as well as in the rivers of the northern Mediterranean borderlands (Magny et al., 2012; Filippidi & De Lange, 2019; Wagner et al., 2019). Our data confirm than the Var river system also counts for the northern Mediterranean borderlands' river systems showing a flow peak during the Holocene insolation maximum. Therefore, while during the time period of the ORL, our data does not indicate high river runoff from the Var system, this latter became highly active during the time period of S1 deposit.

Enhanced river influence also likely explains the large increase in TOC recorded in our core since the end of YD and until 6 ka (Figure 3). At first glance, this time interval of TOC enrichment could characterize the increase in river runoff that triggered the ORL deposit in the deep western Mediterranean (~14.5 – 7 ka, Jimenez-Espejo et al., 2007, 2008).

However, in our record, although TOC record increases from 12 to 8.5 ka (+0.1%), the maximum of accumulation is recorded between 8 and 6 ka (+ 0.2%), after the end of the last ORL event as found in the Alboran and Balearic Seas (Cacho et al., 2002; Rogerson et al., 2008). At our core location, the timing of the accumulation of organic matter is closely linked to the deposit of the eastern sapropel S1 and thus, despite a studied site located in the western Mediterranean, where occurred the last ORL, the core KESC9-14 is mostly affected by the S1 deposit of the eastern basin.

The early TOC increasing trend (12 to 8.5 ka) is concomitant to the rise in relative abundance of the dominant species from PCA Group 2 (e.g. *H. balthica*, *B. inflata* and *G. subglobosa*) and *M. barleeanus* from PCA Group 3, while species from PCA Group 1 dominant during the deglaciation (e.g. *U. mediterranea*) largely decreased over this time period (Figure 6). Such a community turnover might trace a change in the origin/nature of the OM. While during the YD, nutrients sustaining primary production might have originated from the mixing of the water column, we assume that nutrients and organic matter originate mainly from fluvial inputs, conditioning as such the nature of primary producers and with that the nature of OM arriving at the sea floor. According to De Rijk et al. (2000), *U. mediterranea* which is highly abundant during the last deglaciation, is a shallow infaunal species amongst the most opportunistic taxa found in the eutrophic western Mediterranean and is dependent on an important supply of fresh organic matter, with a high nutritious value. *Melonis barleeanus* on the other hand is an intermediate infaunal species of which the distribution in the Mediterranean Sea does not show any clear relationships with labile organic flux levels (De Rijk et al., 2000). This is probably because its natural microhabitat within the sediment is relatively remote from the sediment-water interface where labile organic components are easily available. Moreover, it has been suggested that *Melonis spp*.

feed either on degraded organic components, or on stocks of nitrate reducing bacteria, associated with the successive redox boundaries (e.g. Caralp, 1988; Jorissen, 1999).

However, from ~8.5 to 6 ka, the core records a larger organic matter accumulation, with TOC values reaching up to 0.7%. Synchronously, the plantktic $\delta^{18}O$ becomes gradually heavier, marking perhaps a decrease in the fluvial input, which is coherent with the progressively drier climate on the continent as reported from the Corchia Cave (Figure 8). This feature is accompanied by a major decrease in the proportions of "degraded OM species" *M. barleeanus* in favor of an increase of the "labile OM opportunistic species" *U. mediterranea* (Figure 8), which seems to be coherent with our previous ecological interpretations. Furthermore, the association of *U. mediterranea* with the more mesotrophic species *C. pachyderma* is indicative of less eutrophic benthic environments, which seems to contradict the high values of TOC during this time period. The latter is probably the result of a better preservation (e.g. less oxygenated bottom waters) rather than a high input of organic matter. This is also supported by the overall decreasing trend of benthic $\delta^{13}C$ values from the early Holocene which seems to indicate a progressive installation of a sluggish bottom water circulation, reaching its paroxysmal phase between 7.5 and 5.5 ka (Figure 4).

Geochemical and sedimentological evidences of reduced activity of the LIW were also observed between 9 and 6 ka in the Corsica Trough (Toucanne et al., 2012, Figure 1). These authors further argued that the LIW flux in the Ligurian Sea was largely influenced by its low/ceased formation in the eastern basin during Sapropel 1 event. Although foraminiferal composition and diversity do not show change that may indicate dysoxic environmental conditions, we note the presence of *G. subglobosa* that nearly exclusively occurs at that time (Figure 6). This species is highly abundant in the lower part of the Oxygen Minimum Zone of the Arabian Sea (e.g. Schumacher et al., 2007; Caulle et al., 2014) and has been described as tolerant to relatively low oxygen conditions (bottom water oxygen content = 5–16 μM). These

"low" oxygen conditions might have further been accentuated by more sluggish circulation at that time, leading to the good preservation of the TOC in our sediment record. Interestingly, the benthic $\delta^{13}C$ decreasing pattern in our study core is not regular and is characterized by two phases of minimum values matching the two phases of the sapropel S1 event observed in the Eastern Mediterranean (e.g. Ba/Al, V/Al, Hennekam et al. 2014) and interrupted by a rebound in the $\delta^{13}C$ value between 8-8.5 ka (Figure 4). This latter might be due to a short but significant/dramatic reactivation of the LIW formation during the well-known 8.2 ka cold relapse interrupting the sapropel S1 event (e.g. Rohling et al., 2002, Tachikawa et al., 2015). Similar features were observed in the Sicily Channel (Incarbona and Sprovieri, 2020, Figure 4), with benthic $\delta^{13}C$ records reflecting lower LIW density and weakened seafloor ventilation, all coinciding with the sapropel S1 timing. Thus, we conclude than the organic matter accumulation/preservation at site KESC9-14 between 8.2 and 6 ka, is most likely resulting from the slowdown of the general intermediate oceanic circulation in Mediterranean Sea at the time of Sapropel 1.

Thus, from our core location, the geochemical and sedimentological proxies does not seem to point to major change in the regional hydrology at the time period corresponding to the deposit of the last ORL (14.5- 9 ka). However, following Rohling et al. (2015) the input of alpine melt water through rivers between 15 and 13 ka and 11.5 to 9 ka, that corresponds of intervals of sea level rise (Rogerson et al., 2008) in the western basin, is the trigger to: (i) shallow the depth at which the Bernoulli effect is effective and (ii) to reduce the formation of dense deep water. Those combined effects were thus suggested to explain the onset of the ORL deposit in the deep western basins at around 14.5 ka and its continuation until 9 ka. From those models, without the pulse of alpine melt water, the ORL deposit should have a timing similar to the S1 deposit as its deposit will entirely depend on the transportation of less saline water through the LIW flowing from the eastern basin. Even our data does not support

the enhancement of river flow from the Var system at that time, their model still stands if we consider that the alpine melting waters were provided by the Rhone River.

However, at our core location, a clear change is recorded at the timing of the S1 deposit with evidence of a significant enhancement of the Var river system activity together with a weak LIW. This might imply that rivers from northern Mediterranean borderlands could be significant contributors to the implementation of organic matter input and general water column stratification promoting the S1 deposit. In this hypothesis, and following the logic of the models developed by Rohling et al. (2015), the inputs of fresh water in the western basin during the Holocene insolation maximum might affect the effect of Bernoulli aspiration over the Strait of Sicily enhancing the development of strong stratification in the eastern basin. In such case, the contribution of western Mediterranean rivers to the development of east Mediterranean sapropel should be further considered.

5.3. Mid- to late Holocene (~6 to 1.5 ka) surface and deep-water environmental changes in the Ligurian Sea: evidence of a millennial timescale variability

Since ~6 ka, most of the geochemical and sedimentological proxies from core KESC9-14 show a rather low amplitude changes compared to the 10-6 kyr period and the deglaciation. Benthic foraminiferal faunas however show a high variability, especially in the relative abundances of the dominant species *M. barleeanus* (5 to 30 % contribution of the total fauna, Figure 6) that we previously interpreted as thriving on rather low-quality organic matter from fluvial origin. We are therefore perhaps recording periods of high/low river runoff. However, this foraminiferal variability does not have any solid coherency with the measured environmental proxies, unless for the somewhat negative correlation between the relative abundances of *M. barleeanus* and TOC content from ~8 to 2 ka and a positive

correlation after ~2 ka. This lack of consistency would mean that either: i) there is no direct link between the TOC content in our study core and the fluvial organic matter input to the study area during this time period, ii) the TOC traces organic matter originating from primary production in this overall period of low river runoff compared to the 10-6 kyr period, iii) we are recording mostly changes in the preservation state of the TOC in the sediment that is controlled by bottom water ventilation, and/or iv) the benthic species are responding to a complexity of environmental factors that our dataset fails to highlight.

In spite of our difficulty to link the benthic foraminiferal signal to the measured environmental variables, many of the latter nonetheless (i.e. TOC, D90, benthic $\delta^{13}C$, planktic $\delta^{18}O$) show rather regular millennial-scale changes (Figure 9). Although we are aware that these are mostly low amplitude changes that can be part of the usual noise of such paleorecords, the overall consistency that we observe between several independent proxies from the same core justifies to our opinion the following attempt to uncover the environmental signal hidden behind these changes. First, the TOC content shows several peaks, that are mostly (not all) simultaneous to changes in D90, benthic $\delta^{13}C$ and planktic $\delta^{18}O$, and are mainly centred around 4.3, 3.4, 2.3 and 1.4 ka (cf. yellow bands in Figure 9). Whenever high TOC values are observed, we note an increase in the D90 which is due to increased proportions of fine sands, and a general presence of a bimodal grain size spectrum (Figure 3). The existence of a secondary mode in the grain size distribution around 105-110 μm might indicate a new and stronger hydrodynamic process. A similar process was observed during Holocene cold periods in the French Atlantic coast and was interpreted as the result of increased storminess leading to remobilization of sediments from shallower settings during these overall dry periods on the continent (Sorrel et al., 2012, Durand et al., 2018). In the nearby Gulf of Lion, periods of enhanced storm activity are evidenced by higher content of smectites in the coastal area (Sabatier et al., 2012, Figure 9) and seem to be coherent with our

three recent events of higher D90 values (Figure 9). Additionally, these short episodes of slight increase in sand fraction might also be due to relatively stronger slope current and/or reflect period of high winter storm activity. Indeed, despite overall high benthic $\delta^{13}C$ values since ~6 ka, most likely indicating an overall active intermediate water mass circulation, the benthic $\delta^{13}C$ record show several peaks that are mostly synchronous with D90 peaks, implying perhaps episodes of better ventilated bottom waters (Figure 9). Presently, periods of high/low active intermediate circulation occurs seasonally when a new water mass (the Winter intermediate water, WIW) forms every winter in the Ligurian Sea under strong north westerly winds cooling the surface waters (Lacombe and Tchernia, 1960; Gasparini et al., 1999). We can therefore imagine similar dynamics in the past on longer time periods of enhanced wind activity cooling surface waters of the Ligurian Sea. In our core, the planktic $\delta^{18}O$ record shows 0.5 ‰ shifts that may correspond to periods of slightly colder sea surface temperatures (cf. yellow bands in Figure 9). The presence of active winter winds was suggested to explain the episodes of anomalously cold sea surface temperatures from mid- to late Holocene and thus the production of dense sea water in WM Sea from Alborean to Thyrrenian sub-basins (Cacho et al, 2000, Frigola et al., 2007). These active winds, by mixing the water column, might have triggered primary production, explaining therefore the higher TOC content during these episodes.

Although caution is advised when comparing such rapid events with other records due to the discrepancies in age model constraints, it is interesting to note that some of these "cold" periods seem to be synchronous with the cold events defined from alkenones-SST reconstructions in the Gulf of Lion (6.2, 5.2, 4.1, 2.4, 1.4, and 0.3 ka; Jalali et al., 2016). These authors further linked these episodes to the cold relapse events (CR) identified in the Atlantic Ocean and dated at around 6.3, 4.7, 2.7, 1.7, 0.55 ka (Wanner et al., 2011). It appears therefore, that from the mid- to late Holocene, the Ligurian Sea could have experienced

episodes of relatively active bottom water ventilation, associated with cold surface temperatures that can be linked to active winds triggering primary production by the mixing of the water column, and thus inducing episodes of increased organic flux to the sea floor.

5.4. The embedded multi-centennial to millennial cyclicity: response of the Ligurian Sea to external and internal forcing factors

Time series analyses of independent proxies from core KESC9-14 (benthic and planktic foraminiferal $\delta^{18}O$ and $\delta^{13}C$, foraminiferal relative abundances and XRF ratios Ca/Ti show overall common significant frequencies peaks with specific bottom-surface frequency bands:

The lower frequency band between 2.5-3 kyr is well expressed in all analysed proxies and is present along the entire 15 kyr record (Figure 10). A continuous 2.5 kyr cycle is common in most Holocene paleoclimatic records from the Atlantic (e.g. Dansgaard et al., 1984; O'Brien et al., 1995), from the Aegean Sea in the Eastern Mediterranean (Rohling et al., 2002) and was also reported from the Corchia Cave over the last 13 kyr (Tognarelli et al., 2018). This frequency appears to be related to solar activity and known as the Hallstatt cycle (Hood and Jirikowic, 1990; Dergachev and Chistyakov, 1995; Schatten and Hoyt, 1997; Scafetta et al., 2016) deriving probably from the quasi-rhythmic pattern in the periodic revolution of the planets around the Sun (Scafetta et al., 2016). By modulating the cosmic rays reaching the Earth, it influences the climate and Earth's albedo through the formation of clouds (e.g. Svensmark et al., 2009, 2012; Scafetta et al., 2016).

Our benthic foraminiferal isotopic data record a supplementary frequency peak at1,5-1,6 kyr, mainly present from ~15 and 4 ka. A 1.6 kyr cycle was initially recorded in studies from the Atlantic Ocean (e.g. Bianchi and McCave, 1999; McDermott et al., 1999; Bond et

al., 2001; Moros et al., 2004; Witt and Schumann, 2005) and was also reported from cores in the nearby Gulf of Lion (Azuara et al., 2020). The origin of this cycle was largely debated (Debret 2007; Dima and Lohman, 2009; Soon et al., 2014) and is now preferentially attributed to a likely oceanic-driven internal forcing, at least for the Late Holocene (Broecker et al., 1999; McManus et al., 1999) resulting from the thermohaline sensitivity to the north European meltwater discharge (Debret et al., 2009). A 1.6 kyr cycle was also found in the eastern Mediterranean from benthic foraminiferal time series over the Holocene (Le Houedec et al., 2020). Because this cycle was absent in the planktic record, the authors attributed the 1.6 kyr cycle to either an internal Mediterranean circulation mode or a result from an Atlantic circulation mode. Here also the 1.5-1.6 kyr frequency peak is absent from the planktic stable isotopic record, corroborating perhaps a link with the bottom water larger scale circulation rather than with the climate forcing. On the other hand, the planktic $\delta^{18}O$ record together with most analyzed XRF elemental ratios show periodicity significant frequency peak at 1.1-1.2 kyr, that mostly occurs during the Holocene (Figure 10). Interestingly, from the Corchia Cave, the authors found embedded cyclicities between 1.2 and 1.7 kyr with a 1.2 kyr mode mainly present after 6 ka while the 1.7 kyr peak was seen before 8 ka. A 1.7 kyr cycle was also reported from the vegetation in the WM (Fletcher et al., 2013) before 6 ka and interpreted as a response to the rainfall activity. Therefore, we cannot totally preclude a potential role of a climatic forcing to explain also the 1.6 kyr peak recorded in our data, although in this case, its absence from the planktic record is difficult to reconcile with a climate origin.

We also record periodicities at around 400-500 and 900-1000 yr occurring mainly before and after the 10-6 kyr time period (Figure 10). These multi-centennial periodicities were also reported in WM palaeoclimatological records from Corchia Cave (Tognarelli et al., 2018) and from the eastern basin (Hennekam et al., 2014; Le Houedec et al., 2020). Because these cycles are found in residual atmospheric ^{14}C production data, they were interpreted as

reflecting changes in the strength of the solar activity (e.g. Stuiver and Braziunas, 1993). In the Gulf of Lion, a periodicity around 600-700 years was detected and interpreted as a Pacific tropical feature (Azuara et al., 2020).

The results of these time series analyses confirm that, despite the usual inherent uncertainties to paleorecords, the WM ecological and hydro-sedimentary characteristics are rhythmed by larger-scale ocean-atmosphere processes likely involving Mediterranean-Atlantic climatic teleconnections modes. Further advanced time-domain statistical methods (e.g. cross-coherence analysis) applied on several similar generated time-series from the Mediterranean and other oceanic basins are needed in order to extract the common basin-wide scale periodicities, and to identify specific instances whereby oceanic/atmospheric changes at two geographically disparate locations are related (i.e., teleconnections).

6. Conclusions:

Our WM marine record shows a complex interaction between local processes such as the Var fluvial input controlled by humidity on the continent, basin scale processes implicating the Mediterranean thermohaline circulation and the active/low formation of the LIW in the Eastern Mediterranean, and global processes linked to relative sea-level rise from glacial to interglacial periods.

Our data highlight three distinct time periods characterized by specific hydrological and climatological patterns, all happening in a context of rising sea-level and its consequence on the proximity of our study site to the continent. Our proxy data from the 15-11 kyr time interval are imprinted by global climatic processes characterizing the last deglaciation. While benthic foraminifera abundances indicate an overall eutrophic benthic environments and ventilated bottom waters, grain size analyses and XRF data describe enhanced Var River

input during the B/A time period and lowered fluvial input during the YD. We associated these results to the regional climate literature describing the B/A as a humid and warm period while the YD is described as dry and cold.

The second time period from 11 to 6 ka is characterized by a higher river discharge indicated by all geochemical and sedimentological proxies. responding to more humid climate and we suggested that the bottom environment of the Ligurian Sea also record the slow-down of the LIW. This is translated into the sediment by a change in the benthic community with the dominance of *M. barleeanus* and environmental conditions favouring the preservation of organic matter. This is interpreted as a result of increasing precipitation over the Var River drainage basin. Two phases in the intensity of the river runoff are emphasised by a major change in the benthic community with the dominance of the "refractory OM species" *M. barleeanus* from ~11 to 8 ka and the "opportunistic labile OM species" *U. mediterranea* from ~8 to 6 ka. This might indicate a higher continental input during the first phase, diminishing progressively during the second phase. Meanwhile, the highly depleted benthic ~$\delta^{13}C$ suggests a sluggish intermediate circulation in the Ligurian Sea, causing relatively low oxygen levels in the bottom waters, yet without reaching anoxia or even severe hypoxia as no benthic species indicate such conditions. The timing of this phase and the synchronous re-ventilation around 8 ka with the interruption of Sapropel S1 event in the Eastern Mediterranean suggests a close link with the slowdown of the LIW formation in the Levantine basin during S1.

The last 6 kyr are characterised by overall mesotrophic to eutrophic benthic environments in a context of lower fluvial input compared to the former periods. We hypothesise that the relatively high organic matter fluxes to the sea floor might be due to the activation of coastal and slope upwelling systems once the sea-level rise stabilized. Interestingly, this time period was also marked by short term variations imprinted in several

of our independent geochemical proxies (stable isotopic records, XRF records, TOC record, sedimentology record). The general coherence of these changes with several regional records led us to suggest that these might be related to episodes of more or less active bottom water ventilation linked to changes in the wind activity.

The analyses of the embedded cyclicities in several of our records highlight common frequency peaks with Atlantic and Mediterranean marine records and continental records adjacent to these basins. This might indicate that the Ligurian Sea sediments record larger-scale ocean-atmosphere processes, particularly those linked to Mediterranean-Atlantic climatic teleconnections modes. In order to define the exact nature of these climatic modes, further inter and intra basin high resolution studies are needed to extract this natural variability from sedimentary records.

Acknowledgments:

The postdoctoral fellowship of S. Le Houedec (first author) and the master internship of F. Z. Bouhdayad were funded by France's Regional Council of Pays de la Loire (TANDEM project). The Ifremer center is acknowledged for the financial support of the ESSCAR-9 cruise in 2008. Data analyses of core KESC9-14 have been funded by Institut Carnot Ifremer Edrome (grant A0811101) and by TANDEM project. We warmly thank Joêl Etoubleau for the help in the WD-XRF analyses. Scanning electron microscope (SEM) photographs of foraminifera were performed at the SCIAM (Service Commun d'Imagerie et d'Analyses Microscopiques) platform of the University of Angers (France).

Data Availability:

Datasets related to this article can be found at http://dx.doi.org/10.17632/zvcj85frn8.1, an open-source online data repository hosted at Mendeley Data.

Declaration of interests

☒ The authors declare that they have no known competing financial interests or personal relationships that could have appeared to influence the work reported in this paper.

References:

Abu-Zied, R.H., Rohling, E.J., Jorissen, F.J., Fontanier, C., Casford, J.S.L., Cooke, S., 2008. Benthic foraminiferal response to changes in bottom-water oxygenation and organic carbon flux in the eastern Mediterranean during LGM to Recent times. Marine Micropaleontology 67, 46–68. https://doi.org/10.1016/j.marmicro.2007.08.006

Allen, J.R.M., Huntley, B., 2009. Last Interglacial palaeovegetation, palaeoenvironments and chronology: a new record from Lago Grande di Monticchio, southern Italy. Quaternary Science Reviews 28, 1521–1538. https://doi.org/10.1016/j.quascirev.2009.02.013

Allen, J.R.M., Huntley, B., Watts, W.A., 1996. The vegetation and climate of northwest Iberia over the last 14,000 years. Journal of Quaternary Science 11, 125–147. https://doi.org/10.1002/(SICI)1099-1417(199603/04)11:2<125::AID-JQS232>3.0.CO;2-U

Allen, J.R.M., Watts, W.A., Huntley, B., 2000. Weichselian palynostratigraphy, palaeovegetation and palaeoenvironment; the record from Lago Grande di Monticchio, southern Italy. Quaternary International, EDLP - Med Special 73–74, 91–110. https://doi.org/10.1016/S1040-6182(00)00067-7

Alley, R.B., Meese, D.A., Shuman, C.A., Gow, A.J., Taylor, K.C., Grootes, P.M., White, J.W.C., Ram, M., Waddington, E.D., Mayewski, P.A., Zielinski, G.A., 1993. Abrupt increase in Greenland snow accumulation at the end of the Younger Dryas event. Nature 362, 527–529. https://doi.org/10.1038/362527a0

Angue Minto'o, C.M., Bassetti, M.-A., Toucanne, S., Jouet, G., 2016. Distribution of ostracod and benthic foraminiferal assemblages during the last 550kyr in the East-Corsica basin, western Mediterranean Sea: A paleo-environmental reconstruction. Revue de Micropaléontologie, Ostracides and (Paleo)environments : in memoriam of J.-F. Babinot and J.-P. Colin (2 nd) 59, 83–96. https://doi.org/10.1016/j.revmic.2016.01.002

Ariztegui, D., Asioli, A., Lowe, J.J., Trincardi, F., Vigliotti, L., Tamburini, F., Chondrogianni, C., Accorsi, C.A., Bandini Mazzanti, M., Mercuri, A.M., Van der Kaars, S., McKenzie, J.A., Oldfield, F., 2000. Palaeoclimate and the formation of sapropel S1: inferences from Late Quaternary lacustrine and marine sequences in the central Mediterranean region. Palaeogeography, Palaeoclimatology, Palaeoecology 158, 215–240. https://doi.org/10.1016/S0031-0182(00)00051-1

Astraldi, M., Gasparini, G.P., 1992. The seasonal characteristics of the circulation in the north Mediterranean basin and their relationship with the atmospheric-climatic conditions. Journal of Geophysical Research: Oceans 97, 9531–9540. https://doi.org/10.1029/92JC00114

Azuara, J., Sabatier, P., Lebreton, V., Jalali, B., Sicre, M.A., Dezileau, L., Bassetti, M.A., Frigola, J., Coumbourieu-Nebout, N., 2020. Mid- to Late-Holocene Mediterranean climate variability: Contribution of multi-proxy and multi-sequence comparison using wavelet analysis in the northwestern Mediterranean basin. Earth-Science Reviews 103232. https://doi.org/10.1016/j.earscirev.2020.103232

Bahr, A., Jiménez-Espejo, F.J., Kolasinac, N., Grunert, P., Hernández-Molina, F.J., Röhl, U., Voelker, A.H.L., Escutia, C., Stow, D.A.V., Hodell, D., Alvarez-Zarikian, C.A., 2014. Deciphering bottom current velocity and paleoclimate signals from contourite deposits in the Gulf of Cádiz during the last 140 kyr: An inorganic geochemical approach. Geochemistry, Geophysics, Geosystems 15, 3145–3160. https://doi.org/10.1002/2014GC005356

Bahr, A., Kaboth, S., Jiménez-Espejo, F. J., Sierro, F. J., Voelker, A. H. L., Lourens, L., Röhl, U., Reichart, G.J., Escutia, C., Hernández-Molina, F.J., Pross, J., Friedrich, O., 2015. Persistent monsoonal forcing of Mediterranean Outflow Water dynamics during the late Pleistocene. Geology, 43, 951-954. https://doi.org/10.1130/G37013.1

Bard, E., Delaygue, G., Rostek, F., Antonioli, F., Silenzi, S., Schrag, D.P., 2002. Hydrological conditions over the western Mediterranean basin during the deposition of the cold Sapropel 6 (ca. 175 kyr BP). Earth and Planetary Science Letters 202, 481–494. https://doi.org/10.1016/S0012-821X(02)00788-4

Bassetti, M.-A., Berné, S., Sicre, M. A., Dennielou, B., Alonso, Y., Buscail, R., Jalali, B., Hebert, B., Menniti, C., 2016. Holocene hydrological changes in the Rhône River (NW Mediterranean) as recorded in the marine mud belt. Climate of the Past 12, 1539–1553. https://doi.org/10.5194/cp-12-1539-2016

Berger, A., Loutre, M.F., 1991. Insolation values for the climate of the last 10 million years. Quaternary Science Reviews 10, 297–317. https://doi.org/10.1016/0277-3791(91)90033-Q

Bianchi, G.G., McCave, I.N., 1999. Holocene periodicity in North Atlantic climate and deep-ocean flow south of Iceland. Nature 397, 515–517. https://doi.org/10.1038/17362

Blott, S.J. and Pye, K. (2001) GRADISTAT: a grain size distribution and statistics package for the analysis of unconsolidated sediments. Earth Surface Processes and Landforms 26, 1237-1248

Bond, G., Kromer, B., Beer, J., Muscheler, R., Evans, M.N., Showers, W., Hoffmann, S., Lotti-Bond, R., Hajdas, I., Bonani, G., 2001. Persistent solar influence on North Atlantic climate during the Holocene. Science 294, 2130–2136.

Bonneau, L., Jorry, S.J., Toucanne, S., Jacinto, R.S., Emmanuel, L., 2014. Millennial-Scale Response of a Western Mediterranean River to Late Quaternary Climate Changes: A View from the Deep Sea. The Journal of Geology 122, 687–703. https://doi.org/10.1086/677844

Bonneau, L., Toucanne, S., Bayon, G., Jorry, S.J., Emmanuel, L., Silva Jacinto, R., 2017. Glacial erosion dynamics in a small mountainous watershed (Southern French Alps): A

source-to-sink approach. Earth and Planetary Science Letters 458, 366–379. https://doi.org/10.1016/j.epsl.2016.11.004

Broecker, W.S., Sutherland, S., Peng, T.-H., 1999. A Possible 20th-Century Slowdown of Southern Ocean Deep Water Formation. Science 286, 1132–1135. https://doi.org/10.1126/science.286.5442.1132

Cacho, I., Grimalt, J.O., Canals, M., 2002. Response of the Western Mediterranean Sea to rapid climatic variability during the last 50,000 years: a molecular biomarker approach. Journal of Marine Systems, MATER: MAss Transfer and Ecosystem Response 33–34, 253–272. https://doi.org/10.1016/S0924-7963(02)00061-1

Cacho, I., Grimalt, J.O., Canals, M., Sbaffi, L., Shackleton, N.J., Schönfeld, J., Zahn, R., 2001. Variability of the western Mediterranean Sea surface temperature during the last 25,000 years and its connection with the Northern Hemisphere climatic changes. Paleoceanography 16, 40–52. https://doi.org/10.1029/2000PA000502

Cacho, I., Grimalt, J.O., Pelejero, C., Canals, M., Sierro, F.J., Flores, J.A., Shackleton, N., 1999. Dansgaard-Oeschger and Heinrich event imprints in Alboran Sea paleotemperatures. Paleoceanography 14, 698–705. https://doi.org/10.1029/1999PA900044

Cacho, I., Grimalt, J.O., Sierro, F.J., Shackleton, N., Canals, M., 2000. Evidence for enhanced Mediterranean thermohaline circulation during rapid climatic coolings. Earth and Planetary Science Letters 183, 417–429. https://doi.org/10.1016/S0012-821X(00)00296-X

Caralp, M.-H., 1988. Late glacial to recent deep-sea benthic foraminifera from the northeastern Atlantic (Cadiz Gulf) and western Mediterranean (Alboran Sea): Paleooceanographic results. Marine Micropaleontology 13, 265–289. https://doi.org/10.1016/0377-8398(88)90006-0

Casella, E., Molcard, A., Provenzale, A., 2011. Mesoscale vortices in the Ligurian Sea and their effect on coastal upwelling processes. Journal of Marine Systems, 41st International Liege Colloquium on Ocean Dynamics"Science based management of the coastal waters 88, 12–19. https://doi.org/10.1016/j.jmarsys.2011.02.019

Casford, J.S.L., Rohling, E.J., Abu-Zied, R., Cooke, S., Fontanier, C., Leng, M., Lykousis, V., 2002. Circulation changes and nutrient concentrations in the late Quaternary Aegean Sea: A nonsteady state concept for sapropel formation. Paleoceanography 17, 14-1-14–11. https://doi.org/10.1029/2000PA000601

Casford, J.S.L., Rohling, E.J., Abu-Zied, R.H., Fontanier, C., Jorissen, F.J., Leng, M.J., Schmiedl, G., Thomson, J., 2003. A dynamic concept for eastern Mediterranean circulation and oxygenation during sapropel formation. Palaeogeography, Palaeoclimatology, Palaeoecology 190, 103–119. https://doi.org/10.1016/S0031-0182(02)00601-6

Caulle, C., Koho, K.A., Mojtahid, M., Reichart, G.J., Jorissen, F.J., 2014. Live (Rose Bengal stained) foraminiferal faunas from the northern Arabian Sea: faunal succession within and below the OMZ. Biogeosciences 11, 1155–1175. https://doi.org/10.5194/bg-11-1155-2014

Cauwet, G., 1981. Chapter 4 Non-Living Particulate Matter, in: Duursma, E.K., Dawson, R. (Eds.), Elsevier Oceanography Series, Marine Organic Chemistry. Elsevier, pp. 71–89. https://doi.org/10.1016/S0422-9894(08)70326-X

Ciobanu, M.-C., Rabineau, M., Droz, L., Révillon, S., Ghiglione, J.-F., Dennielou, B., Jorry, S.J., Kallmeyer, J., Etoubleau, J., Pignet, P., Crassous, P., Vandenabeele-Trambouze, O., Laugier, J., Guégan, M., Godfroy, A., Alain, K., 2012. Sedimentological imprint on subseafloor microbial communities in Western Mediterranean Sea Quaternary sediments. Biogeosciences 9, 3491–3512. https://doi.org/10.5194/bg-9-3491-2012

Combourieu Nebout, N., Bout-Roumazeilles, V., Dormoy, I., Peyron, O., 2009. Events of persistent dryness in the Mediterranean throughout the last 50 000 years. Science et changements planétaires / Sécheresse 20, 210–216. https://doi.org/10.1684/sec.2009.0181

Combourieu Nebout, N., Londeix, L., Baudin, F., Turon, J.L., Von Grafenstein, U., Zahn, R., 1999. Quaternary marine and continental paleoenvironments in the western Mediterranean (Site 976, Alboran Sea): palynological evidence, in: Proceeding of ODP Scientific Results. edited by: Zahn, R., Comas, M. C., and Klaus, A, College Station, TX (Ocean Drilling Program), pp. 457–468.

Combourieu-nebout, N., Paterne, M., Turon, J.-L., Siani, G., 1998. A high-resolution record of the Last Deglaciation in the Central Mediterranean Sea: paleovegetation and paleohydrological evolution. Quaternary Science Reviews 17, 303–317. https://doi.org/10.1016/S0277-3791(97)00039-5

Dansgaard, W., Johnsen, S.J., Clausen, H.B., Dahl-Jensen, D., Gundestrup, N., Hammer, C.U., Oeschger, H., 1984. North Atlantic Climatic Oscillations Revealed by Deep Greenland Ice Cores, in: Climate Processes and Climate Sensitivity. American Geophysical Union (AGU), pp. 288–298. https://doi.org/10.1029/GM029p0288

De Lange, G.J., Thomson, J., Reitz, A., Slomp, C.P., Speranza Principato, M., Erba, E., Corselli, C., 2008. Synchronous basin-wide formation and redox-controlled preservation of a Mediterranean sapropel. Nature Geoscience 1, 606–610. https://doi.org/10.1038/ngeo283

De Rijk, S., Jorissen, F.J., Rohling, E.J., Troelstra, S.R., 2000. Organic flux control on bathymetric zonation of Mediterranean benthic foraminifera. Marine Micropaleontology 40, 151–166. https://doi.org/10.1016/S0377-8398(00)00037-2

Debret, M., Bout-Roumazeilles, V., Grousset, F., Desmet, M., McManus, J.F., Massei, N., Sebag, D., Petit, J.-R., Copard, Y., Trentesaux, A., 2007. The origin of the 1500-year climate cycles in Holocene North-Atlantic records. Climate of the Past 3, 569–575. https://doi.org/10.5194/cp-3-569-2007

Debret, M., Sebag, D., Costra, X., Massei, N., Petit, J.R., Chapron, E., Bout-Roumazeilles, V., 2009. Evidence from wavelet analysis for a mid-Holocene transition in global climate forcing. Quaternary Science Reviews 28, 2675–2688. https://doi.org/10.1016/j.quascirev.2009.06.005

Dergachev, V. and Chistyakov, V., 1995. Cosmogenic Radiocarbon and Cyclical Natural Processes. Radiocarbon 37, 417–424. https://doi.org/10.1017/S0033822200030897

Dima, M., Lohmann, G., 2009. Conceptual model for millennial climate variability: a possible combined solar-thermohaline circulation origin for the ~1,500-year cycle. Clim Dyn 32, 301–311. https://doi.org/10.1007/s00382-008-0471-x

Dixit, Y., Toucanne, S., Lora, J.M., Fontanier, C., Pasquier, V., Bonnin, L., Jouet, G., Tripati, A., 2020. Enhanced western Mediterranean rainfall during past interglacials driven by North Atlantic pressure changes. Climate of the Past Discussions 1–28. https://doi.org/10.5194/cp-2019-75

Dubar, M., Anthony, E.J., 1995. Holocene Environmental Change and River-Mouth Sedimentation in the Baie des Anges, French Riviera. Quaternary Research 43, 329–343. https://doi.org/10.1006/qres.1995.1039

Durand, M., Mojtahid, M., Maillet, G.M., Baltzer, A., Schmidt, S., Blet, S., Marchès, E., Howa, H., 2018. Late Holocene record from a Loire River incised paleovalley (French inner continental shelf): Insights into regional and global forcing factors. Palaeogeography, Palaeoclimatology, Palaeoecology 511, 12–28. https://doi.org/10.1016/j.palaeo.2018.06.035

El Maghraoui, M., Joron, J.-L., Etoubleau, J., Cambon, P., Treuil, M., 1999. Determination of Forty Four Major and Trace Elements in GPMA Magmatic Rock Reference Materials using X-ray Fluorescence Spectrometry (XRF) and Instrumental Neutron Activation Analysis (INAA). Geostandards Newsletter 23, 59–68. https://doi.org/10.1111/j.1751-908X.1999.tb00559.x

Emeis, K., Struck, U., Schulz, H.-M., Rosenberg, R., Bernasconi, S., Erlenkeuser, H., Sakamoto, T., Martinez-Ruiz, F., 2000. Temperature and salinity variations of Mediterranean Sea surface waters over the last 16,000 years from records of planktonic stable oxygen isotopes and alkenone unsaturation ratios. Palaeogeography, Palaeoclimatology, Palaeoecology 158, 259–280. https://doi.org/10.1016/S0031-0182(00)00053-5

Filippidi, A., Lange, G.J.D., 2019. Eastern Mediterranean Deep Water Formation During Sapropel S1: A Reconstruction Using Geochemical Records Along a Bathymetric Transect in the Adriatic Outflow Region. Paleoceanography and Paleoclimatology 34, 409–429. https://doi.org/10.1029/2018PA003459

Fletcher, W.J., Debret, M., Goñi, M.F.S., 2013. Mid-Holocene emergence of a low-frequency millennial oscillation in western Mediterranean climate: Implications for past dynamics of the North Atlantic atmospheric westerlies. The Holocene 23, 153–166. https://doi.org/10.1177/0959683612460783

Fletcher, W.J., Sánchez Goñi, M.F., 2008. Orbital- and sub-orbital-scale climate impacts on vegetation of the western Mediterranean basin over the last 48,000 yr. Quaternary Research 70, 451–464. https://doi.org/10.1016/j.yqres.2008.07.002

Fontanier, C., Jorissen, F.J., Chaillou, G., David, C., Anschutz, P., Lafon, V., 2003. Seasonal and interannual variability of benthic foraminiferal faunas at 550m depth in the Bay of Biscay. Deep Sea Research Part I: Oceanographic Research Papers 50, 457–494. https://doi.org/10.1016/S0967-0637(02)00167-X

Frigola, J., Moreno, A., Cacho, I., Canals, M., Sierro, F.J., Flores, J.A., Grimalt, J.O., Hodell, D.A., Curtis, J.H., 2007. Holocene climate variability in the western Mediterranean region from a deepwater sediment record. Paleoceanography 22. https://doi.org/10.1029/2006PA001307

Garcia, J., Mojtahid, M., Howa, H., Michel, E., Schiebel, R., Charbonnier, C., Anschutz, P., Jorissen, F.J., 2013. Benthic and Planktic Foraminifera as Indicators of Late Glacial to Holocene Paleoclimatic Changes in a Marginal Environment: An Example from the Southeastern Bay of Biscay. Acta Protozoologica 52.

Gasparini, G.P., Zodiatis, G., Astraldi, M., Galli, C., Sparnocchia, S., 1999. Winter intermediate water lenses in the Ligurian Sea. Journal of Marine Systems 20, 319–332. https://doi.org/10.1016/S0924-7963(98)00089-X

Giorgi, F., 2006. Climate change hot-spots. Geophysical Research Letters 33. https://doi.org/10.1029/2006GL025734

Goineau, A., Fontanier, C., Jorissen, F.J., Lansard, B., Buscail, R., Mouret, A., Kerhervé, P., Zaragosi, S., Ernoult, E., Artéro, C., Anschutz, P., Metzger, E., Rabouille, C., 2011. Live (stained) benthic foraminifera from the Rhône prodelta (Gulf of Lion, NW Mediterranean): Environmental controls on a river-dominated shelf. Journal of Sea Research 65, 58–75. https://doi.org/10.1016/j.seares.2010.07.007

Goudeau, M.-L.S., Grauel, A.-L., Tessarolo, C., Leider, A., Chen, L., Bernasconi, S.M., Versteegh, G.J.M., Zonneveld, K.A.F., Boer, W., Alonso-Hernandez, C.M., De Lange, G.J., 2014. The Glacial–Interglacial transition and Holocene environmental changes in sediments from the Gulf of Taranto, central Mediterranean. Marine Geology 348, 88–102. https://doi.org/10.1016/j.margeo.2013.12.003

Grimm, R., Maier-Reimer, E., Mikolajewicz, U., Schmiedl, G., Müller-Navarra, K., Adloff, F., Grant, K.M., Ziegler, M., Lourens, L.J., Emeis, K.-C., 2015. Late glacial initiation of Holocene eastern Mediterranean sapropel formation. Nature Communications 6, 7099. https://doi.org/10.1038/ncomms8099

Hammer, Ø., Harper, D.A.T., Ryan, P.D., 2001. PAST: Paleontological statistics software package for education and data analysis. Palaeontologia Electronica 4, 9 pp.

Hennekam, R., Jilbert, T., Schnetger, B., Lange, G.J. de, 2014. Solar forcing of Nile discharge and sapropel S1 formation in the early to middle Holocene eastern Mediterranean. Paleoceanography 29, 343–356. https://doi.org/10.1002/2013PA002553

Higgs, N.C., Thomson, J., Wilson, T.R.S., Croudace, I.W., 1994. Modification and complete removal of eastern Mediterranean sapropels by postdepositional oxidation. Geology 22, 423–426. https://doi.org/10.1130/0091-7613(1994)022<0423:MACROE>2.3.CO;2

Hood, L.L. and Jirikowic, J.L., 1990. Recurring variations of probable solar origin in the atmospheric Δ14C time record. Geophysical Research Letters 17, 85–88. https://doi.org/10.1029/GL017i001p00085

Incarbona, A., Sprovieri, M., 2020. The Postglacial Isotopic Record of Intermediate Water Connects Mediterranean Sapropels and Organic-Rich Layers. Paleoceanography and Paleoclimatology 35, e2020PA004009. https://doi.org/10.1029/2020PA004009

Jalali, B., Sicre, M.-A., Bassetti, M.-A., Kallel, N., 2016. Holocene climate variability in the North-Western Mediterranean Sea (Gulf of Lion). Climate of the Past 12, 91–101. https://doi.org/10.5194/cp-12-91-2016

Jalali, B., Sicre, M.-A., Klein, V., Schmidt, S., Maselli, V., Lirer, F., Bassetti, M.-A., Toucanne, S., Jorry, S.J., Insinga, D.D., Petrosino, P., Châles, F., 2018. Deltaic and Coastal Sediments as Recorders of Mediterranean Regional Climate and Human Impact Over the Past Three Millennia. Paleoceanography and Paleoclimatology 33, 579–593. https://doi.org/10.1029/2017PA003298

Jimenez-Espejo, F.J., Martinez-Ruiz, F., Sakamoto, T., Iijima, K., Gallego-Torres, D., Harada, N., 2007. Paleoenvironmental changes in the western Mediterranean since the last glacial maximum: High resolution multiproxy record from the Algero–Balearic basin. Palaeogeography, Palaeoclimatology, Palaeoecology 246, 292–306. https://doi.org/10.1016/j.palaeo.2006.10.005

Jimenez-Espejo, F.J., Martinez-Ruiz, F., Rogerson, M., González-Donoso, J.M., Romero, O.E., Linares, D., Sakamoto, T., Gallego-Torres, D., Ruiz, J.L.P., Ortega-Huertas, M., Claros, J.A.P., 2008. Detrital input, productivity fluctuations, and water mass circulation in the westernmost Mediterranean Sea since the Last Glacial Maximum. Geochemistry, Geophysics, Geosystems 9. https://doi.org/10.1029/2008GC002096

Jorissen, F.J., 1999. Benthic foraminiferal microhabitats below the sediment-water interface. In: Modern Foraminifera. Springer, Dordrecht. https://doi.org/10.1007/0-306-48104-9_10

Jorissen, F.J., Barmawidjaja, D.M., Puskaric, S., van der Zwaan, G.J., 1992. Vertical distribution of benthic foraminifera in the northern Adriatic Sea: The relation with the organic flux. Marine Micropaleontology, Approaches to Paleoproductivity Reconstructions 19, 131–146. https://doi.org/10.1016/0377-8398(92)90025-F

Jorry, S.J., Jégou, I., Emmanuel, L., Silva Jacinto, R., Savoye, B., 2011. Turbiditic levee deposition in response to climate changes: The Var Sedimentary Ridge (Ligurian Sea). Marine Geology 279, 148–161. https://doi.org/10.1016/j.margeo.2010.10.021

Juza, M., Escudier, R., Vargas-Yañez, M., Mourre, B., Heslop, E., Allen, J., Tintoré, J., 2019. Characterization of changes in Western Intermediate Water properties enabled by an innovative geometry-based detection approach. Journal of Marine Systems 191, 1–12. https://doi.org/10.1016/j.jmarsys.2018.11.003

Juza, M., Renault, L., Ruiz, S., Tintoré, J., 2013. Origin and pathways of Winter Intermediate Water in the Northwestern Mediterranean Sea using observations and numerical simulation. Journal of Geophysical Research: Oceans 118, 6621–6633. https://doi.org/10.1002/2013JC009231

Kallel, N., Duplessy, J.-C., Labeyrie, L., Fontugne, M., Paterne, M., Montacer, M., 2000. Mediterranean pluvial periods and sapropel formation over the last 200 000 years. Palaeogeography, Palaeoclimatology, Palaeoecology 157, 45–58. https://doi.org/10.1016/S0031-0182(99)00149-2

Kandiano, E.S., Bauch, H.A., Fahl, K., 2014. Last interglacial surface water structure in the western Mediterranean (Balearic) Sea: Climatic variability and link between low and high latitudes. Global and Planetary Change 123, 67–76. https://doi.org/10.1016/j.gloplacha.2014.10.004

Kerckhove, C., Barfety, J.-C., Bogdanoff, S., Lemoine, M., Bureau de recherches géologiques et minières . Service géologique national, 1980. Carte géologique de la France à 1/250 000.

Kidd, R.B., Cita, M.B., and Ryan, W.B.F., 1978. Stratigraphy of eastern Mediterranean sapropel sequences recovered during Leg 42A and their paleoenvironmental significance. In Hsu, K.J., and Montadert, L. (eds.), Initial Reports of the Deep-Sea Drilling Project. U.S. Government Printing Office, pp. 421–443.

Kotthoff, U., Müller, U.C., Pross, J., Schmiedl, G., Lawson, I.T., Schootbrugge, B. van de, Schulz, H., 2008a. Lateglacial and Holocene vegetation dynamics in the Aegean region: an integrated view based on pollen data from marine and terrestrial archives: The Holocene. https://doi.org/10.1177/0959683608095573

Kotthoff, U., Pross, J., Müller, U.C., Peyron, O., Schmiedl, G., Schulz, H., Bordon, A., 2008b. Climate dynamics in the borderlands of the Aegean Sea during formation of sapropel S1 deduced from a marine pollen record. Quaternary Science Reviews 27, 832–845. https://doi.org/10.1016/j.quascirev.2007.12.001

Kotthoff, U., Pross, J., Müller, U.C., Peyron, O., Schmiedl, G., Schulz, H., Bordon, A., 2008c. Palynomorphs from the Lateglacial and Holocene of the Mt-Athos Basin, Aegean Sea. https://doi.org/10.1594/PANGAEA.830178

Kuhnt, T., Schmiedl, G., Ehrmann, W., Hamann, Y., Hemleben, C., 2007. Deep-sea ecosystem variability of the Aegean Sea during the past 22 kyr as revealed by Benthic Foraminifera. Marine Micropaleontology 64, 141–162. https://doi.org/10.1016/j.marmicro.2007.04.003

Lacombe, H., Tchernia, P., 1960. Quelques traits généraux de l'hydrologie Méditerranéenne. Cahiers Océanographiques 12, 527–547.

Lambeck, K., Bard, E., 2000. Sea-level change along the French Mediterranean coast for the past 30 000 years. Earth and Planetary Science Letters 175, 203–222. https://doi.org/10.1016/S0012-821X(99)00289-7

Le Houedec, S., Mojtahid, M., Bicchi, E., Lange, G.J. de, Hennekam, R., 2020. Suborbital Hydrological Variability Inferred From Coupled Benthic and Planktic Foraminiferal-Based Proxies in the Southeastern Mediterranean During the Last 19 ka. Paleoceanography and Paleoclimatology 35, e2019PA003827. https://doi.org/10.1029/2019PA003827

Lionello, P., Malanotte-Rizzoli, P., Boscolo, R., Alpert, P., Artale, V., Li, L., Luterbacher, J., May, W., Trigo, R., Tsimplis, M., Ulbrich, U., Xoplaki, E., 2006. The Mediterranean climate: An overview of the main characteristics and issues, in: Lionello, P., Malanotte-Rizzoli, P., Boscolo, R. (Eds.), Developments in Earth and Environmental Sciences, Mediterranean. Elsevier, pp. 1–26. https://doi.org/10.1016/S1571-9197(06)80003-0

Lourens, L.J., Antonarakou, A., Hilgens, F.J., Van Hoof, A.A., Vernaud-Grazzini, C., Zachariasse, W.J., 1996. Evaluation of the plio-Pleistocene astronomical timescale. Paleoceanography 11, 391–413.

Magny, M. and Bégeot, C., 2004. Hydrological changes in the European midlatitudes associated with freshwater outbursts from Lake Agassiz during the Younger Dryas event and

the early Holocene. Quaternary Research 61, 181–192. https://doi.org/10.1016/j.yqres.2003.12.003

Magny, M., Combourieu-Nebout, N., de Beaulieu, J.L., Bout-Roumazeilles, V., Colombaroli, D., Desprat, S., Francke, A., Joannin, S., Ortu, E., Peyron, O., Revel, M., Sadori, L., Siani, G., Sicre, M.A., Samartin, S., Simonneau, A., Tinner, W., Vannière, B., Wagner, B., Zanchetta, G., Anselmetti, F., Brugiapaglia, E., Chapron, E., Debret, M., Desmet, M., Didier, J., Essallami, L., Galop, D., Gilli, A., Haas, J.N., Kallel, N., Millet, L., Stock, A., Turon, J.L., Wirth, S., 2013. North and South palaeohydrological contrasts in the central Mediterranean during the Holocene: tentative synthesis and working hypotheses. Climate of the Past 9, 2043–2071. https://doi.org/10.5194/cp-9-2043-2013

Magny, M., Joannin, S., Galop, D., Vannière, B., Haas, J.N., Bassetti, M., Bellintani, P., Scandolari, R., Desmet, M., 2012. Holocene palaeohydrological changes in the northern Mediterranean borderlands as reflected by the lake-level record of Lake Ledro, northeastern Italy. Quaternary Research 77, 382–396. https://doi.org/10.1016/j.yqres.2012.01.005

Marino, G., Rohling, E.J., Sangiorgi, F., Hayes, A., Casford, J.L., Lotter, A.F., Kucera, M., Brinkhuis, H., 2009. Early and middle Holocene in the Aegean Sea: interplay between high and low latitude climate variability. Quaternary Science Reviews 28, 3246–3262. https://doi.org/10.1016/j.quascirev.2009.08.011

Martinez-Ruiz, F., Kastner, M., Gallego-Torres, D., Rodrigo-Gámiz, M., Nieto-Moreno, V., Ortega-Huertas, M., 2015. Paleoclimate and paleoceanography over the past 20,000 yr in the Mediterranean Sea Basins as indicated by sediment elemental proxies. Quaternary Science Reviews 107, 25–46. https://doi.org/10.1016/j.quascirev.2014.09.018

Marullo, S., Salusti, E., Viola, A., 1985. Observations of a small-scale baroclinic eddy in the Ligurian Sea. Deep Sea Research Part A. Oceanographic Research Papers 32, 215–222. https://doi.org/10.1016/0198-0149(85)90029-9

Mas, V., Mulder, T., Dennielou, B., Schmidt, S., Khripounoff, A., Savoye, B., 2010. Multiscale spatio-temporal variability of sedimentary deposits in the Var turbidite system (North-Western Mediterranean Sea). Marine Geology 275, 37–52. https://doi.org/10.1016/j.margeo.2010.04.006

McCulloch, M., Taviani, M., Montagna, P., López Correa, M., Remia, A., Mortimer, G., 2010. Proliferation and demise of deep-sea corals in the Mediterranean during the Younger Dryas. Earth and Planetary Science Letters 298, 143–152. https://doi.org/10.1016/j.epsl.2010.07.036

McDermott, F., Frisia, S., Huang, Y., Longinelli, A., Spiro, B., Heaton, T.H.E., Hawkesworth, C.J., Borsato, A., Keppens, E., Fairchild, I.J., van der Borg, K., Verheyden, S., Selmo, E., 1999. Holocene climate variability in Europe: Evidence from δ18O, textural and extension-rate variations in three speleothems. Quaternary Science Reviews 18, 1021–1038. https://doi.org/10.1016/S0277-3791(98)00107-3

McManus, J.F., Oppo, D.W., Cullen, J.L., 1999. A 0.5-Million-Year Record of Millennial-Scale Climate Variability in the North Atlantic. Science 283, 971–975. https://doi.org/10.1126/science.283.5404.971

Meese, D.A., Gow, A.J., Alley, R.B., Zielinski, G.A., Grootes, P.M., Ram, M., Taylor, K.C., Mayewski, P.A., Bolzan, J.F., 1997. The Greenland Ice Sheet Project 2 depth-age scale: Methods and results. Journal of Geophysical Research: Oceans 102, 26411–26423. https://doi.org/10.1029/97JC00269

Mercone, D., Thomson, J., Abu-Zied, R.H., Croudace, I.W., Rohling, E.J., 2001. High-resolution geochemical and micropalaeontological profiling of the most recent eastern Mediterranean sapropel. Marine Geology 177, 25–44. https://doi.org/10.1016/S0025-3227(01)00122-0

Meyers, P.A., Arnaboldi, M., 2005. Trans-Mediterranean comparison of geochemical paleoproductivity proxies in a mid-Pleistocene interrupted sapropel. Palaeogeography, Palaeoclimatology, Palaeoecology 222, 313–328. https://doi.org/10.1016/j.palaeo.2005.03.020

Migeon, S., Mulder, T., Savoye, B., Sage, F., 2006. The Var turbidite system (Ligurian Sea, northwestern Mediterranean)—morphology, sediment supply, construction of turbidite levee and sediment waves: implications for hydrocarbon reservoirs. Geo-Marine Letters 26, 361. https://doi.org/10.1007/s00367-006-0047-x

Millot, C., 2009. Another description of the Mediterranean Sea outflow. Progress in Oceanography 82, 101–124. https://doi.org/10.1016/j.pocean.2009.04.016

Millot, C., 1999. Circulation in the Western Mediterranean Sea. Journal of Marine Systems 20, 423–442. https://doi.org/10.1016/S0924-7963(98)00078-5

Millot, C., 1990. The Gulf of Lion' hydrodynamics. Continental Shelf Research, France-JGOFS, ECOMARGE Particle Fluxes and Ecosystem Response on a Continental Margin 10, 885–894. https://doi.org/10.1016/0278-4343(90)90065-T

Millot, C., 1987. The circulation of the Levantine Intermediate Water in the Algerian Basin. Journal of Geophysical Research: Oceans 92, 8265–8276. https://doi.org/10.1029/JC092iC08p08265

Millot, C. and Taupier-Letage, I., 2005. Circulation in the Mediterranean Sea, in: Saliot, A. (Ed.), The Mediterranean Sea, Handbook of Environmental Chemistry. Springer Berlin Heidelberg, Berlin, Heidelberg, pp. 29–66. https://doi.org/10.1007/b107143

Mojtahid, M., Durand, M., Coste, P.-O., Toucanne, S., Howa, H., Nizou, J., Eynaud, F., Penaud, A., 2018. Millennial-scale Holocene hydrological changes in the northeast Atlantic: New insights from 'La Grande Vasière' mid-shelf mud belt: The Holocene. https://doi.org/10.1177/0959683618816478

Mojtahid, M., Jorissen, F.J., Garcia, J., Schiebel, R., Michel, E., Eynaud, F., Gillet, H., Cremer, M., Diz Ferreiro, P., Siccha, M., Howa, H., 2013. High resolution Holocene record in the southeastern Bay of Biscay: Global versus regional climate signals. Palaeogeography, Palaeoclimatology, Palaeoecology 377, 28–44. https://doi.org/10.1016/j.palaeo.2013.03.004

Mojtahid, M., Manceau, R., Schiebel, R., Hennekam, R., Lange, G.J. de, 2015. Thirteen thousand years of southeastern Mediterranean climate variability inferred from an integrative planktic foraminiferal-based approach. Paleoceanography 30, 402–422. https://doi.org/10.1002/2014PA002705

Moros, M., Emeis, K., Risebrobakken, B., Snowball, I., Kuijpers, A., McManus, J., Jansen, E., 2004. Sea surface temperatures and ice rafting in the Holocene North Atlantic: climate influences on northern Europe and Greenland. Quaternary Science Reviews, Holocene climate variability - a marine perspective 23, 2113–2126. https://doi.org/10.1016/j.quascirev.2004.08.003

Mulder, T., Savoye, B., Syvitski, J., Parize, O., 1997. Des courants de turbidité hyperpycnaux dans la tête du canyon du Var ? Données hydrologiques et observations de terrain. Oceanologica Acta.

Munsell, A.H., 1912. A Pigment Color System and Notation. The American Journal of Psychology 23, 236–244. https://doi.org/10.2307/1412843

Murat, A., 1991. Enregistrement sédimentaire des paléoenvironnements quaternaires en Méditerranée orientale (PhD thesis). Université de Perpignan. France

Murat, A., 1999. Pliocene–Pleistocene occurrence of sapropels in the Western Mediterranean Sea and their relation to eastern Mediterranean sapropels. R. Zahn, M.C. Comas, A. Klaus (Eds.), Proc. ODP, Sci. Results, vol. 161, Ocean Drilling Program), College Station, TX , pp. 519-527, 10.2973/odp.proc.sr.161.244.1999

Naughton, F., Sanchez Goñi, M.F., Desprat, S., Turon, J. L., Duprat, J., Malaizé, B., Joli, C., Cortijo, E., Drago, T., Freitas, M.C., 2007. Present-day and past (last 25000 years) marine pollen signal off western Iberia. Marine Micropaleontology 62, 91–114. https://doi.org/10.1016/j.marmicro.2006.07.006

O'Brien, S.R., Mayewski, P.A., Meeker, L.D., Meese, D.A., Twickler, M.S., Whitlow, S.I., 1995. Complexity of Holocene Climate as Reconstructed from a Greenland Ice Core. Science 270, 1962–1964. https://doi.org/10.1126/science.270.5244.1962

Pasquier, V., Revillon, S., Leroux, E., Molliex, S., Mocochain, L., Rabineau, M., 2019. Quantifying Biogenic Versus Detrital Carbonates on Marine Shelf: An Isotopic Approach. Front. Earth Sci. 7. https://doi.org/10.3389/feart.2019.00164

Pautot, G., 1981. Cadre morphologique de la Baie des Anges (Nice-Côte d'Azur) : modèle d'instabilité de pente continentale. Oceanologica Acta 4, 203-211

Pérez-Asensio, J.N., Frigola, J., Pena, L.D., Sierro, F.J., Reguera, M.I., Rodríguez-Tovar, F.J., Dorador, J., Asioli, A., Kuhlmann, J., Huhn, K., Cacho, I., 2020. Changes in western Mediterranean thermohaline circulation in association with a deglacial Organic Rich Layer formation in the Alboran Sea. Quaternary Science Reviews 228, 106075. https://doi.org/10.1016/j.quascirev.2019.106075

Pèrez-Obiol, R., Julià, R., 1994. Climatic Change on the Iberian Peninsula Recorded in a 30,000-Yr Pollen Record from Lake Banyoles. Quaternary Research 41, 91–98. https://doi.org/10.1006/qres.1994.1010

Petrenko, A.A., 2003. Variability of circulation features in the Gulf of Lion NW Mediterranean Sea. Importance of inertial currents. Oceanologica Acta 26, 323–338. https://doi.org/10.1016/S0399-1784(03)00038-0

Pinot, J.-M. and Ganachaud, A., 1999. The role of winter intermediate waters in the spring-summer circulation of the Balearic Sea: 1. Hydrography and inverse box modeling. Journal of Geophysical Research: Oceans 104, 29843–29864. https://doi.org/10.1029/1999JC900202

Piper, D.J.W. and Savoye, B., 1993. Processes of late Quaternary turbidity current flow and deposition on the Var deep-sea fan, north-west Mediterranean Sea. Sedimentology 40, 557–582. https://doi.org/10.1111/j.1365-3091.1993.tb01350.x

R Core Team, 2013. R: A language and environment for statistical computing. R foundation for statistical computing 1, 409

Regattieri, E., Zanchetta, G., Drysdale, R.N., Isola, I., Hellstrom, J.C., Dallai, L., 2014. Lateglacial to Holocene trace element record (Ba, Mg, Sr) from Corchia Cave (Apuan Alps, central Italy): paleoenvironmental implications. Journal of Quaternary Science 29, 381–392. https://doi.org/10.1002/jqs.2712

Regattieri, E., Zanchetta, G., Isola, I., Zanella, E., Drysdale, R.N., Hellstrom, J.C., Zerboni, A., Dallai, L., Tema, E., Lanci, L., Costa, E., Magrì, F., 2019. Holocene Critical Zone dynamics in an Alpine catchment inferred from a speleothem multiproxy record: disentangling climate and human influences. Scientific Reports 9, 17829. https://doi.org/10.1038/s41598-019-53583-7

Reimer, P.J., Austin, W.E.N., Bard, E., Bayliss, A., Blackwell, P.G., Ramsey, C.B., Butzin, M., Cheng, H., Edwards, R.L., Friedrich, M., Grootes, P.M., Guilderson, T.P., Hajdas, I., Heaton, T.J., Hogg, A.G., Hughen, K.A., Kromer, B., Manning, S.W., Muscheler, R., Palmer, J.G., Pearson, C., Reimer, R.W., Richards, D.A., Scott, E.M., Southon, J.R., Turney, C.S.M., Wacker, L., Adolphi, F., Büntgen, U., Capano, M., Fahrni, S.M., Fogtmann-Schultz, A., Friedrich, R., Köhler, P., Kudsk, S., Miyake, F., Olsen, J., Reining, F., Sakamoto, M., Sookdeo, A. and Talamo, S., 2020. The IntCal20 Northern Hemisphere Radiocarbon Age Calibration Curve (0–55 cal kBP). Radiocarbon 62, 725–757. https://doi.org/10.1017/RDC.2020.41

Richter, T.O., Gaast, S. van der, Koster, B., Vaars, A., Gieles, R., Stigter, H.C. de, Haas, H.D., Weering, T.C.E. van, 2006. The Avaatech XRF Core Scanner: technical description and applications to NE Atlantic sediments. Geological Society, London, Special Publications 267, 39–50. https://doi.org/10.1144/GSL.SP.2006.267.01.03

Rodrigo-Gámiz, M., Martínez-Ruiz, F., Jiménez-Espejo, F.J., Gallego-Torres, D., Nieto-Moreno, V., Romero, O., Ariztegui, D., 2011. Impact of climate variability in the western Mediterranean during the last 20,000 years: oceanic and atmospheric responses. Quaternary Science Reviews 30, 2018–2034. https://doi.org/10.1016/j.quascirev.2011.05.011

Rogerson, M., Cacho, I., Jimenez-Espejo, F., Reguera, M.I., Sierro, F.J., Martinez-Ruiz, F., Frigola, J., Canals, M., 2008. A dynamic explanation for the origin of the western Mediterranean organic-rich layers. Geochemistry, Geophysics, Geosystems 9. https://doi.org/10.1029/2007GC001936

Rohling, E.J., 1994. Review and new aspects concerning the formation of eastern Mediterranean sapropels. Marine Geology 122, 1–28. https://doi.org/10.1016/0025-3227(94)90202-X

Rohling, E.J., Cane, T.R., Cooke, S., Sprovieri, M., Bouloubassi, I., Emeis, K.C., Schiebel, R., Kroon, D., Jorissen, F.J., Lorre, A., Kemp, A.E.S., 2002. African monsoon variability during the previous interglacial maximum. Earth and Planetary Science Letters 202, 61–75. https://doi.org/10.1016/S0012-821X(02)00775-6

Rohling, E.J., Hayes, A., Rijk, S.D., Kroon, D., Zachariasse, W.J., Eisma, D., 1998. Abrupt cold spells in the northwest Mediterranean. Paleoceanography 13, 316–322. https://doi.org/10.1029/98PA00671

Rohling, E.J., Hilgen, F.J., 1991. The eastern Mediterranean climate at times of sapropel formation: a review. Netherlands Journal of Geosciences 70, 253–264.

Rohling, E.J., Jorissen, F.J., De Stigter, H.C., 1997. 200 Year interruption of Holocene sapropel formation in the Adriatic Sea. Journal of Micropalaeontology 16, 97–108. https://doi.org/10.1144/jm.16.2.97

Rohling, E.J., Jorissen, F.J., Grazzini, C.V., Zachariasse, W.J., 1993. Northern Levantine and Adriatic Quaternary planktic foraminifera; Reconstruction of paleoenvironmental gradients. Marine Micropaleontology 21, 191–218. https://doi.org/10.1016/0377-8398(93)90015-P

Rohling, E.J., Marino, G., Grant, K.M., 2015. Mediterranean climate and oceanography, and the periodic development of anoxic events (sapropels). Earth-Science Reviews 143, 62–97. https://doi.org/10.1016/j.earscirev.2015.01.008

Rossignol-Strick, M., 1985. Mediterranean Quaternary sapropels, an immediate response of the African monsoon to variation of insolation. Palaeogeography, Palaeoclimatology, Palaeoecology 49, 237–263. https://doi.org/10.1016/0031-0182(85)90056-2

Rossignol-Strick, M., Nesteroff, W., Olive, P., Vergnaud-Grazzini, C., 1982. After the deluge: Mediterranean stagnation and sapropel formation. Nature 295, 105. https://doi.org/10.1038/295105a0

Sabatier, P., Dezileau, L., Colin, C., Briqueu, L., Bouchette, F., Martinez, P., Siani, G., Raynal, O., Von Grafenstein, U., 2012. 7000years of paleostorm activity in the NW Mediterranean Sea in response to Holocene climate events. Quaternary Research 77, 1–11. https://doi.org/10.1016/j.yqres.2011.09.002

Sage, L., 1976. La sédimentation à l'embouchure d'un fleuve côtier méditerranéen: le Var. Université de Nice, phD thesis, Nice.

Salat, J. and Font, J., 1987. Water mass structure near and offshore the Catalan coast during the winters of 1982 and 1983. Annales geophysicae. Series B. Terrestrial and planetary physics 5, 48–54.

Santoleri, R., Salusti, E., Stocchino, C., 1983. Hydrological currents in the Ligurian Sea. Il Nuovo Cimento C 6, 353–370. https://doi.org/10.1007/BF02507094

Savoye, B., Piper, D.J.W., Droz, L., 1993. Plio-Pleistocene evolution of the Var deep-sea fan off the French Riviera. Marine and Petroleum Geology 10, 550–571. https://doi.org/10.1016/0264-8172(93)90059-2

Scafetta, N., Milani, F., Bianchini, A., Ortolani, S., 2016. On the astronomical origin of the Hallstatt oscillation found in radiocarbon and climate records throughout the Holocene. Earth-Science Reviews 162, 24–43. https://doi.org/10.1016/j.earscirev.2016.09.004

Schatten, K.H. and Hoyt, D.V., 1997. The Role of the Sun in Climate Change. Oxford University Press USA, New York.

Schmiedl, G., de Bovée, F., Buscail, R., Charrière, B., Hemleben, C., Medernach, L., Picon, P., 2000. Trophic control of benthic foraminiferal abundance and microhabitat in the bathyal Gulf of Lion, western Mediterranean Sea. Marine Micropaleontology 40, 167–188. https://doi.org/10.1016/S0377-8398(00)00038-4

Schmiedl, G., Mitschele, A., Beck, S., Emeis, K.-C., Hemleben, C., Schulz, H., Sperling, M., Weldeab, S., 2003. Benthic foraminiferal record of ecosystem variability in the eastern Mediterranean Sea during times of sapropel S5 and S6 deposition. Palaeogeography, Palaeoclimatology, Palaeoecology 190, 139–164. https://doi.org/10.1016/S0031-0182(02)00603-X

Schmiedl, G., Kuhnt, T., Ehrmann, W., Emeis, K.-C., Hamann, Y., Kotthoff, U., Dulski, P., Pross, J., 2010. Climatic forcing of eastern Mediterranean deep-water formation and benthic ecosystems during the past 22 000 years. Quaternary Science Reviews 29, 3006–3020. https://doi.org/10.1016/j.quascirev.2010.07.002

Schumacher, S., Jorissen, F.J., Dissard, D., Larkin, K.E., Gooday, A.J., 2007. Live (Rose Bengal stained) and dead benthic foraminifera from the oxygen minimum zone of the Pakistan continental margin (Arabian Sea). Marine Micropaleontology 62, 45–73. https://doi.org/10.1016/j.marmicro.2006.07.004

Soon, W., Velasco Herrera, V.M., Selvaraj, K., Traversi, R., Usoskin, I., Chen, C.-T.A., Lou, J.-Y., Kao, S.-J., Carter, R.M., Pipin, V., Severi, M., Becagli, S., 2014. A review of Holocene solar-linked climatic variation on centennial to millennial timescales: Physical processes, interpretative frameworks and a new multiple cross-wavelet transform algorithm. Earth-Science Reviews 134, 1–15. https://doi.org/10.1016/j.earscirev.2014.03.003

Sorrel, P., Debret, M., Billeaud, I., Jaccard, S.L., McManus, J.F., Tessier, B., 2012. Persistent non-solar forcing of Holocene storm dynamics in coastal sedimentary archives. Nature Geoscience 5, 892–896. https://doi.org/10.1038/ngeo1619

Sparnocchia, S., Manzella, G.M.R., La Violette, P.E., 2013. The Interannual and Seasonal Variability of the MAW and LIW Core Properties in the Western Mediterranean Sea, in: Seasonal and Interannual Variability of the Western Mediterranean Sea. American Geophysical Union (AGU), pp. 177–194. https://doi.org/10.1029/CE046p0117

Sparnocchia, S., Picco, P., Manzella, G., Ribotti, A., Copello, S., Brasey, P., 1995. Intermediate water formation in the Ligurian Sea. Oceanologica Acta 18, 151–162.

Stuiver, M., Braziunas, T.F., 1993. Modeling Atmospheric 14C Influences and 14C Ages of Marine Samples to 10,000 BC. Radiocarbon 35, 137–189. https://doi.org/10.1017/S0033822200013874

Svensmark, H., Bondo, T., Svensmark, J., 2009. Cosmic ray decreases affect atmospheric aerosols and clouds. Geophysical Research Letters 36. https://doi.org/10.1029/2009GL038429

Svensmark, J., Enghoff, M.B., Svensmark, H., 2012. Effects of cosmic ray decreases on cloud microphysics. Atmospheric Chemistry and Physics Discussions 12, 3595–3617. https://doi.org/10.5194/acpd-12-3595-2012

Tachikawa, K., Vidal, L., Cornuault, M., Garcia, M., Pothin, A., Sonzogni, C., Bard, E., Menot, G., Revel, M., 2015. Eastern Mediterranean Sea circulation inferred from the conditions of S1 sapropel deposition. Climate of the Past 11, 855–867. https://doi.org/10.5194/cp-11-855-2015

Thomson, J., Higgs, N.C., Wilson, T.R.S., Croudace, I.W., De Lange, G.J., Van Santvoort, P.J.M., 1995. Redistribution and geochemical behaviour of redox-sensitive elements around S1, the most recent eastern Mediterranean sapropel. Geochimica et Cosmochimica Acta 59, 3487–3501. https://doi.org/10.1016/0016-7037(95)00232-O

Tjallingii, R., Röhl, U., Kölling, M., Bickert, T., 2007. Influence of the water content on X-ray fluorescence core-scanning measurements in soft marine sediments. Geochemistry, Geophysics, Geosystems 8. https://doi.org/10.1029/2006GC001393

Tognarelli, A., Zanchetta, G., Regattieri, E., Isola, I., Drysdale, R.N., Bini, M., Hellstrom, J.C., 2018. Wavelet analysis of δ18O and δ13C time-series from an Holocene speleothem record from Corchia Cave (central Italy): insights for the recurrence of dry-wet periods in the Central Mediterranean. IJG 137, 128–137. https://doi.org/10.3301/IJG.2017.21

Toucanne, S., Jouet, G., Ducassou, E., Bassetti, M.-A., Dennielou, B., Angue Minto'o, C.M., Lahmi, M., Touyet, N., Charlier, K., Lericolais, G., Mulder, T., 2012. A 130,000-year record of Levantine Intermediate Water flow variability in the Corsica Trough, western Mediterranean Sea. Quaternary Science Reviews 33, 55–73. https://doi.org/10.1016/j.quascirev.2011.11.020

Toucanne, S., Soulet, G., Freslon, N., Silva Jacinto, R., Dennielou, B., Zaragosi, S., Eynaud, F., Bourillet, J.-F., Bayon, G., 2015. Millennial-scale fluctuations of the European Ice Sheet at the end of the last glacial, and their potential impact on global climate. Quaternary Science Reviews 123, 113–133. https://doi.org/10.1016/j.quascirev.2015.06.010

Trigo, I.F., Bigg, G.R., Davies, T.D., 2002. Climatology of Cyclogenesis Mechanisms in the Mediterranean. Mon. Wea. Rev. 130, 549–569. https://doi.org/10.1175/1520-0493(2002)130<0549:COCMIT>2.0.CO;2

Turco, M., Palazzi, E., Von Hardenberg, J., Provenzale, A., 2015. Observed climate change hotspots. Geophysical Research Letters 42, 3521–3528. https://doi.org/10.1002/2015GL063891

Van Santvoort, P.J.M., de Lange, G.J., Thomson, J., Cussen, H., Wilson, T.R.S., Krom, M.D., Ströhle, K., 1996. Active post-depositional oxidation of the most recent sapropel (S1) in sediments of the eastern Mediterranean Sea. Geochimica et Cosmochimica Acta 60, 4007–4024. https://doi.org/10.1016/S0016-7037(96)00253-0

Van Santvoort, P.J.M., Lange, G.J. de, Langereis, C.G., Dekkers, M.J., Paterne, M., 1997. Geochemical and paleomagnetic evidence for the occurrence of "missing" sapropels in eastern Mediterranean sediments. Paleoceanography 12, 773–786.

Wagner, B., Vogel, H., Francke, A., Friedrich, T., Donders, T., Lacey, J.H., Leng, M.J., Regattieri, E., Sadori, L., Wilke, T., Zanchetta, G., Albrecht, C., Bertini, A., Combourieu-Nebout, N., Cvetkoska, A., Giaccio, B., Grazhdani, A., Hauffe, T., Holtvoeth, J., Joannin, S., Jovanovska, E., Just, J., Kouli, K., Kousis, I., Koutsodendris, A., Krastel, S., Lagos, M., Leicher, N., Levkov, Z., Lindhorst, K., Masi, A., Melles, M., Mercuri, A.M., Nomade, S., Nowaczyk, N., Panagiotopoulos, K., Peyron, O., Reed, J.M., Sagnotti, L., Sinopoli, G., Stelbrink, B., Sulpizio, R., Timmermann, A., Tofilovska, S., Torri, P., Wagner-Cremer, F., Wonik, T., Zhang, X., 2019. Mediterranean winter rainfall in phase with African monsoons during the past 1.36 million years. Nature 573, 256–260. https://doi.org/10.1038/s41586-019-1529-0

Wanner, H., Solomina, O., Grosjean, M., Ritz, S.P., Jetel, M., 2011. Structure and origin of Holocene cold events. Quaternary Science Reviews 30, 3109–3123. https://doi.org/10.1016/j.quascirev.2011.07.010

Weldeab, S., Menke, V., Schmiedl, G., 2014. The pace of East African monsoon evolution during the Holocene. Geophysical Research Letters 41, 1724–1732. https://doi.org/10.1002/2014GL059361

Weltje, G.J., Tjallingii, R., 2008. Calibration of XRF core scanners for quantitative geochemical logging of sediment cores: Theory and application. Earth and Planetary Science Letters 274, 423–438. https://doi.org/10.1016/j.epsl.2008.07.054

Witt, A., Schumann, A.Y., 2005. Holocene climate variability on millennial scales recorded in Greenland ice cores. Nonlinear Processes in Geophysics 12, 345–352. https://doi.org/10.5194/npg-12-345-2005

Woerther, P., 2008. ESSCAR-9 cruise, R/V Le Suroît, https://doi.org/10.17600/8020060

Xoplaki, E., González-Rouco, J.F., Luterbacher, J., Wanner, H., 2004. Wet season Mediterranean precipitation variability: influence of large-scale dynamics and trends. Climate Dynamics 23, 63–78. https://doi.org/10.1007/s00382-004-0422-0

Zanchetta, G., Drysdale, R.N., Hellstrom, J.C., Fallick, A.E., Isola, I., Gagan, M.K., Pareschi, M.T., 2007. Enhanced rainfall in the Western Mediterranean during deposition of sapropel S1: stalagmite evidence from Corchia cave (Central Italy). Quaternary Science Reviews 26, 279–286. https://doi.org/10.1016/j.quascirev.2006.12.003

Table 1: **Age models of the sediment core KESC91-14**. Raw radiocarbon ages have been calibrated using (Bchron package; R Core Team, 2013) with IntCal20 marine calibration curve (Reimer et al., 2020) and with a local reservoir age correction (400 ± 50 yr). Samples labelled "Poz-" and "Beta-" were measured respectively at the Poznan Radiocarbon Laboratory (Poland) and at the Beta Analytic Radiocarbon Dating Laboratory (Florida, USA).

Figure 1: Regional Map. a. Map of the Western Mediterranean basin showing the location of the main paleorecords discussed in the text: the lagoon core PB06 (43°30' N; 3°52' E, Sabatier et al., 2012) and the marine core KSGC-31 (43°0'23" N; 3°17'56" E, 60 m water depth; Jalali et al., 2016) from the Gulf of Lion, the marine cores MD01-2472 and MD01-2434 from Corsica Trough (respectively located at 42°36'42" N; 9°43'97" W; 501 m water depth and 42°22'51" N; 9°47'04"E; 780 m water depth, Toucanne et al., 2012) from the Ligurian Sea and the speleothem record from Corchia cave (43°59' N; 10°13' E, Zanchetta et al., 2007). The blue dashed arrows show the main pathway of the intermediate water mass (Levantine Intermediate Water) and the green arrows show the surface current/Northern Current (Millot and Taupier Letage, 2005). The blue circles represent the convection areas where deep water masses are formed. **b.** Detailed map (adapted from Jorry et al., 2011) focused on the study area and showing the Var drainage basin as well as the bathymetric features of the sampled sediment core KESC9-14.

Figure 2: Age model and sediment accumulation rate (SAR) of core KESC9-14. Age model was calculated using IntCal20 curve in Bchron R package (R Core Team, 2013). The Sapropel 1 event was reported as defined by Hennekam et al. (2014) in the Eastern Mediterranea. The last ORL was defined in western Mediterranean from ~14.5 to 9-8 ka by Cacho et al., 2002 but can be regionally prolongated until 7 ka (Incarbona and Sprovieri, 2020).

Figure 3: Organic carbon, XRF data and sedimentological analyses of core KESC9-14. From the bottom to the top are presented age plots of: Sand, silt and clay proportions in the

sediments, grain size distribution of selected representative samples, grain size parameters (D50 and D90), percentages of WD XRF – SiO_2, TiO_2 and CaO, XRF elemental ratio Ln(Ca/Ti) and Total organic carbon content (TOC). For Ln(Ca/Ti) the tick black curves represent the 5-points moving average. The relative sea level (RSL) curve is the predicted sea-level change along the Côte d'Azur (Western Mediterranean) from Lambeck and Bard (2000). The vertical black arrows on the right side indicate the main environmental interpretations (cf. text for details). B/A: Bölling/Allerod, YD: Younger Dryas, the two grey shaded areas are the two phases of Sapropel 1 event (S1a & S1b) as defined by Henrickam et al. (2014) and the ORL time period such as defined by Cacho et al., 2002 (onset) and Incarbona and Sprovieri, 2020 (ending) in western Mediterranean. The yellow bands highlight the short events of the Holocene as discussed in the text (section 5. 3) and the blue stars represent the North Atlantic cold events reported by Wanner et al., 2011. Hol. = Holocene.

Figure 4: Stable isotopic records from core KESC9-14. Age plots of benthic (*C. pachyderma*) and planktic (*G. bulloiaes*) $\delta^{13}C$ and $\delta^{18}O$ records from core KESC9-14 along with their environmental interpretations. Note that the values of $\delta^{18}O$ are in inverse order to match the conventional Glacial-Interglacial marine isotopic reading. For *G. bulloides* $\delta^{18}O$ and $\delta^{13}C$, the tick black curves represent the 3-point moving average. The main events and climate phases are reported similarly to Figure 2.

Figure 5: PCA analysis and mean relative abundance records of benthic foraminifera PCA groups. a. PCA analysis of the main benthic foraminiferal species (i.e. present with ≥5% in at least one sample). The colours represent the four foraminiferal groups identified with the variance analyses (Figure 5b). **b.** Variance analyses of the relative foraminiferal

abundance records. This was calculated for each abundance spectrum as the normalized deviation to the mean in % and presented according to time on a circle. The four cardinal points on the circle are the age (cal kyr BP), the inner circle lines mark the calculated deviation to the mean in % and along the circle the mean value by time quarter (the value is in blue where it is maximal). The deviation to the mean in % of each abundance spectrum by time quarter spectrum was reported below the circles such as it corresponds from the first (left) to the fourth (right) quarter. The groups were constituted by clustering the species with the maximum of their variance in the same time quarter. **c.** Age plots of the mean relative abundance spectra calculated for each of the PCA benthic species groups defined in Figure 5c together with diversity Shannon index *H*. The main events and climate phases are reported similarly to Figure 2.

Figure 6: Relative abundances (%) of the main benthic foraminifera species (occurrence of ≥5% in at least one sample). The four foraminiferal groups correspond to groups determined from PCA and variance analyses (Figure 5). The main events and climate phases are reported similarly to Figure 2.

Figure 7. Scanning electron microscope (SEM) images of benthic foraminifera from Core KESC9–14

Figure 8: Comparison of selected proxies from core KESC9-14 with regional temperature and humidity proxies. From bottom to top, we present: the planktic $\delta^{18}O$, the relative abundances of *U. mediterranea* and *M. barleeanus*, the TOC content from the studied KESC9-14 core and the $\delta^{18}O$ record from Corchia cave (Zanchetta et al., 2007), the humidity index reconstructed from Corchia Cave (North Italy, Regattierri et al., 2019), sea surface

temperature reconstruction from alkenones measurements done on core KSGC-31 (Jalali et al., 2016, Figure1), and June insolation at 15°N (Berger & Loutre, 1991),. The main events and climate phases are reported similarly to Figure 2.

Figure 9: Main features of the Holocene record from core KESC9-14 and comparison with nearby data. From bottom to top, we present a storm index obtained from the sediment composition of PB06 core (Sabatier et al., 2012) collected from a lagoon in the Gulf of Lion and the planktic $\delta^{18}O$, benthic $\delta^{13}C$, D90 and TOC content from our studied KESC9-14 core. The main events and climate phases are reported similarly to Figure 2.

Figure 10: Spectral analyses of main proxies used in core KESC9-14. a. Wavelets analyses of planktic and benthic stable isotopic data from core KESC9-14. **b**. Wavelets analyses of selected XRF proxies from core KESC9-14. The lines mark the 95% confidence level (p=0.05). **c**. Graphic representing the compilation of REDFIT analyses based on the relative abundance records of the 21 main benthic foraminifera species. The blue line marking the mean REDFIT spectrum.

Highlights

- Benthic foraminifera assemblages in the Western Mediterranean over the last 15 kyr
- Benthic environment response to past sub-orbital climate variability
- Impact of the Eastern Mediterranean LIW dynamic on the Ligurian bottom environment
- Active bottom water ventilation under Late Holocene cooler climate episodes

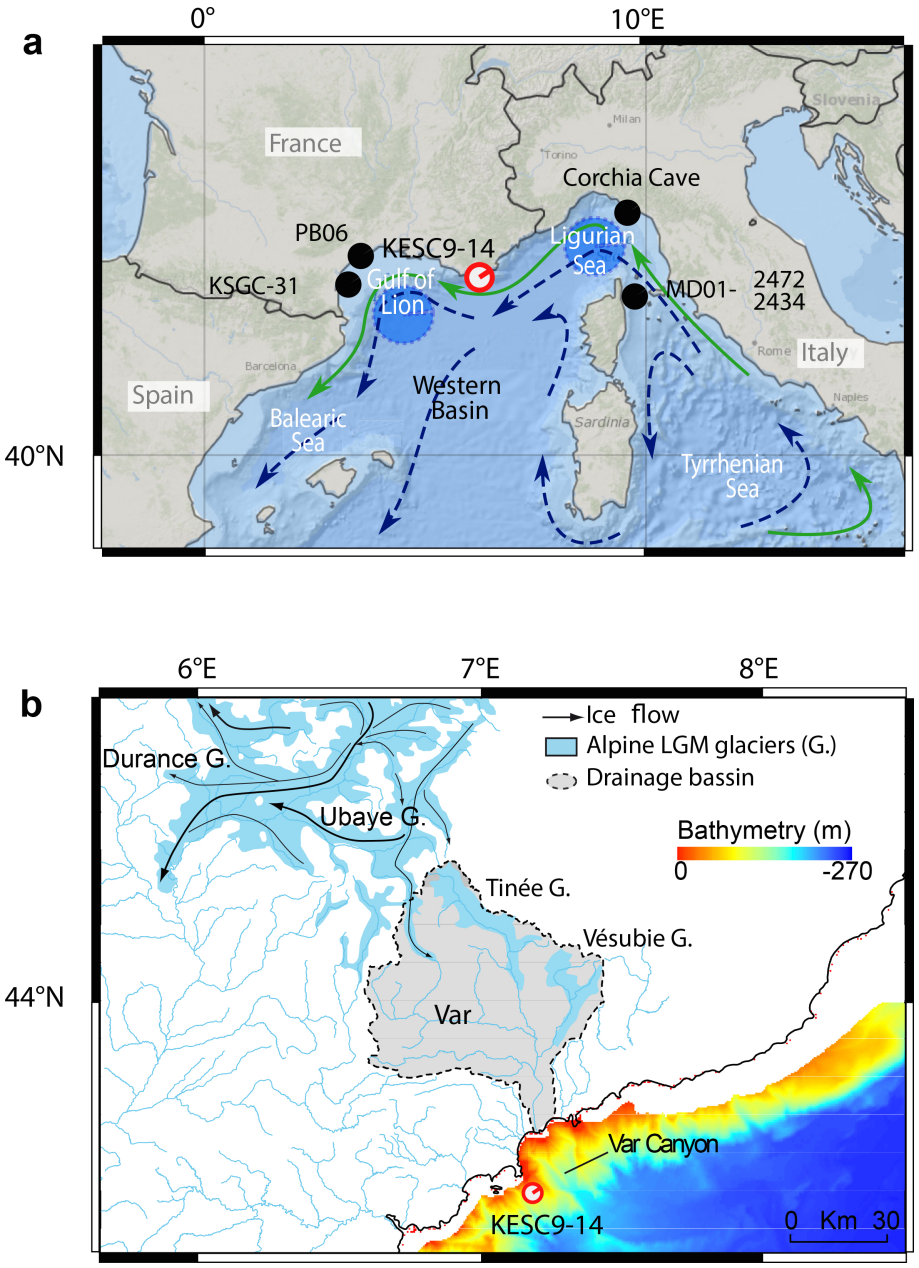
a
0°
10°E
40°N
France
Slovenia
Milan
Torino
Corchia Cave
PB06
KESC9-14
Ligurian Sea
KSGC-31
Gulf of Lion
MD01-2472
2434
Rome
Italy
Barcelona
Spain
Western Basin
Balearic Sea
Sardinia
Naples
Tyrrhenian Sea
b
6°E
7°E
8°E
44°N
Ice flow
Alpine LGM glaciers (G.)
Drainage bassin
Bathymetry (m)
0
-270
Durance G.
Ubaye G.
Tinée G.
Vésubie G.
Var
Var Canyon
KESC9-14
0 Km 30

Figure 1

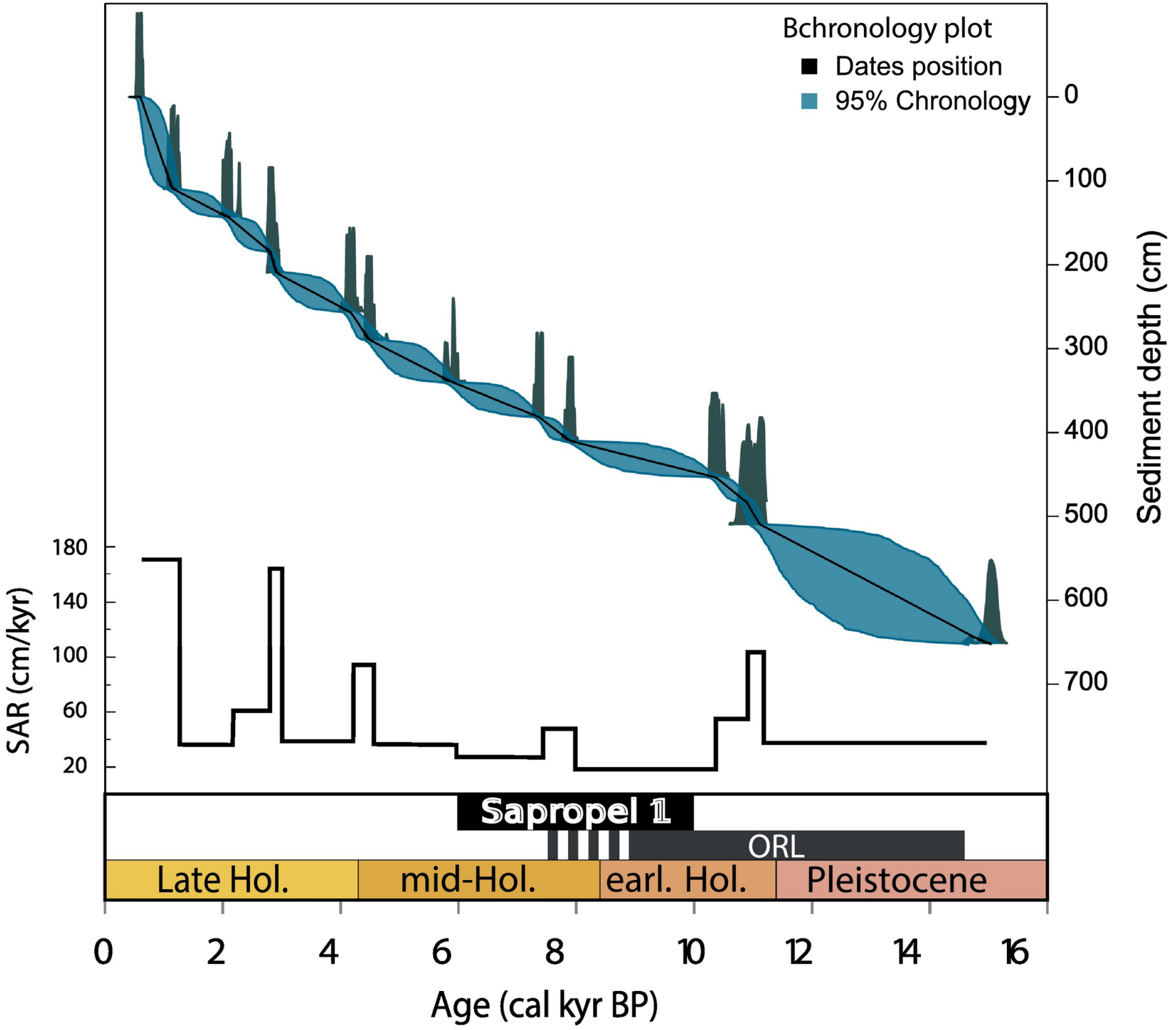
Bchronology plot
Dates position
95% Chronology
0
100
200
300
400
500
600
700
Sediment depth (cm)
180
140
100
60
20
SAR (cm/kyr)
Sapropel 1
ORL
Late Hol.
mid-Hol.
earl. Hol.
Pleistocene
0
2
4
6
8
10
12
14
16
Age (cal kyr BP)

Figure 2

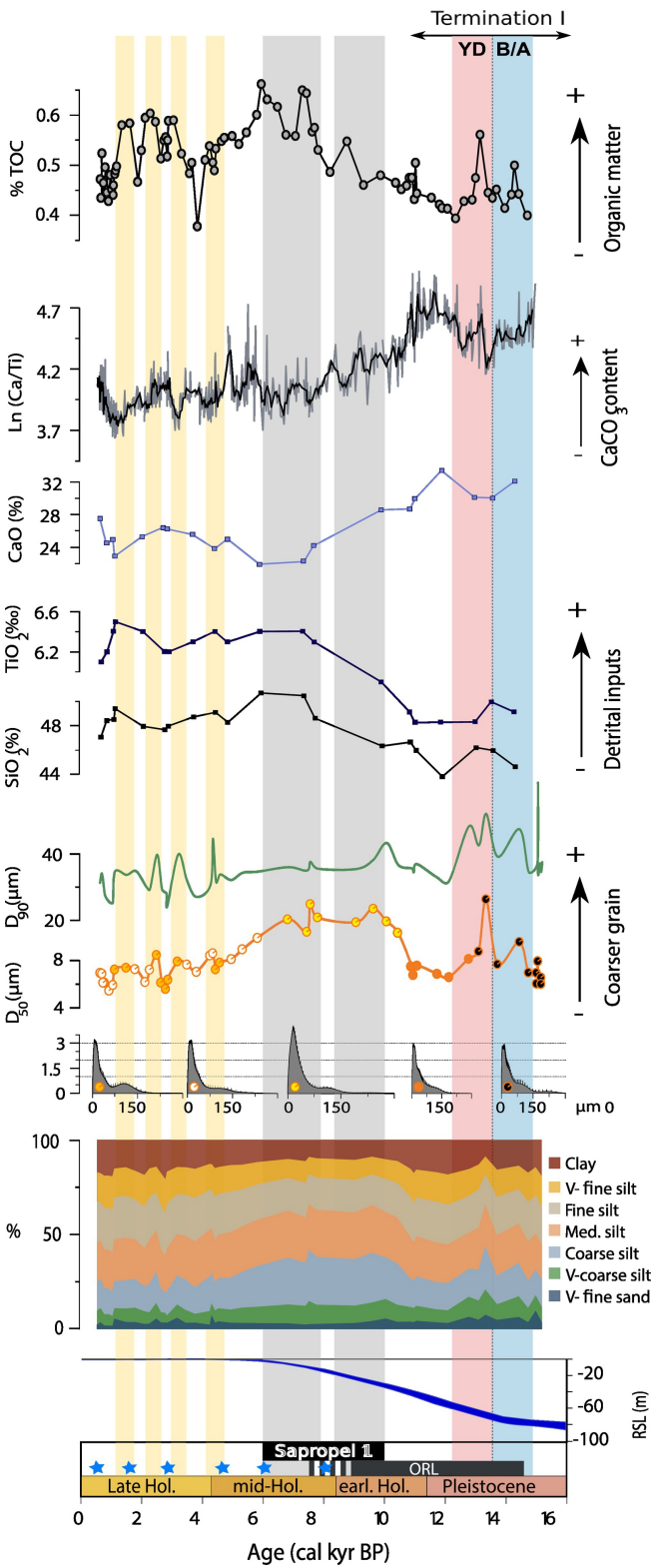
Termination I
YD
B/A
% TOC
0.6
0.5
0.4
Organic matter
Ln (Ca/Ti)
4.7
4.2
3.7
CaCO3 content
CaO (%)
32
28
24
TiO2 (‰)
6.6
6.2
SiO2 (%)
48
44
Detrital inputs
D90(µm)
40
20
D50(µm)
8
4
3
1.5
0
0 150
µm 0
Coarser grain
100
50
%
Clay
V- fine silt
Fine silt
Med. silt
Coarse silt
V-coarse silt
V- fine sand
-20
-60
-100
RSL (m)
Sapropel 1
ORL
Late Hol.
mid-Hol.
earl. Hol.
Pleistocene
0
2
4
6
8
10
12
14
16
Age (cal kyr BP)

Figure 3

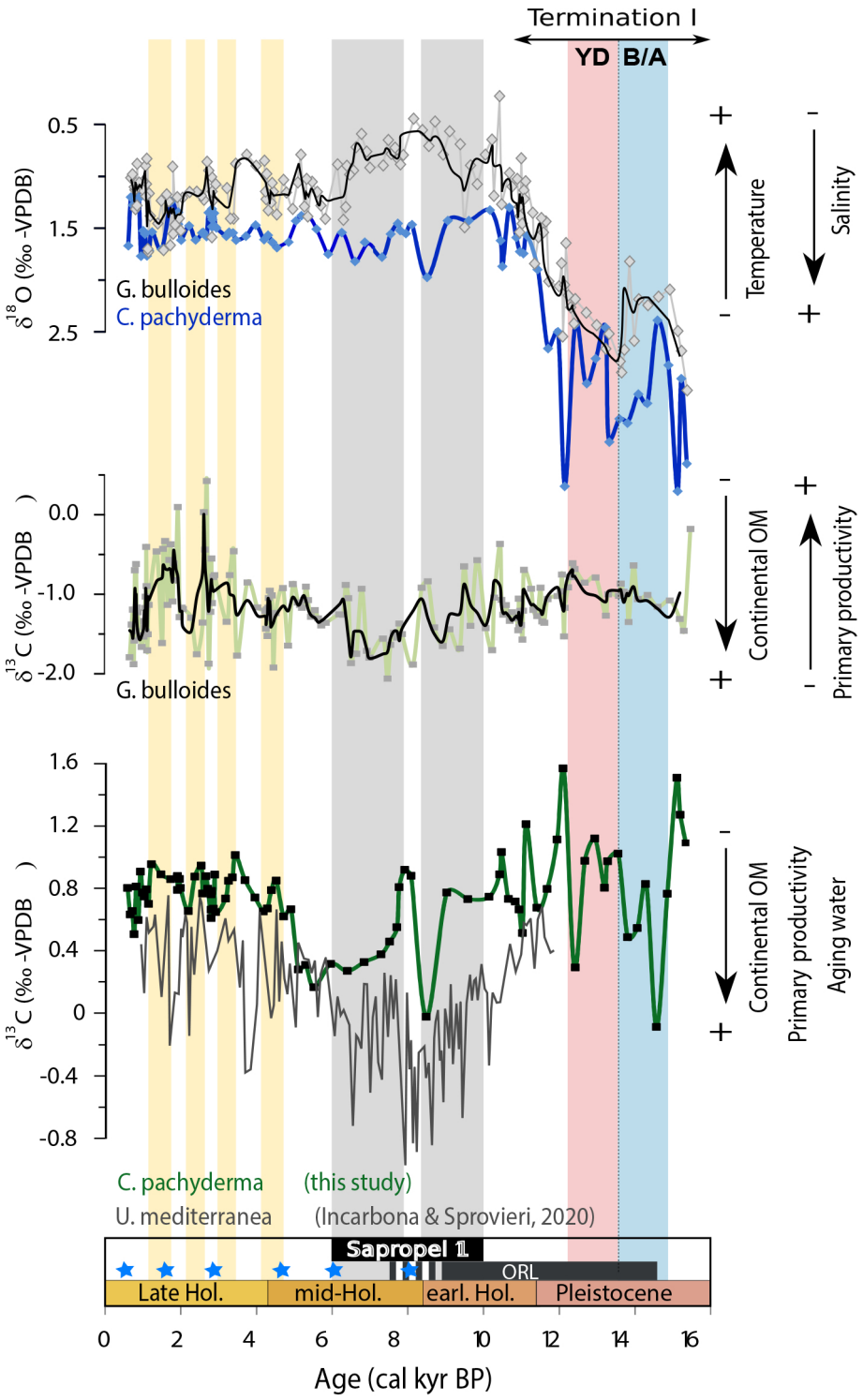
Termination I
YD
B/A
0.5
1.5
2.5
δ18O (‰ -VPDB)
G. bulloides
C. pachyderma
+
-
Temperature
-
+
Salinity
0.0
-1.0
-2.0
δ13C (‰ -VPDB)
G. bulloides
-
+
Continental OM
+
-
Primary productivity
1.6
1.2
0.8
0.4
0
-0.4
-0.8
δ13C (‰ -VPDB)
-
+
Continental OM
Primary productivity
Aging water
C. pachyderma (this study)
U. mediterranea (Incarbona & Sprovieri, 2020)
Sapropel 1
ORL
Late Hol.
mid-Hol.
earl. Hol.
Pleistocene
0
2
4
6
8
10
12
14
16
Age (cal kyr BP)

Figure 4

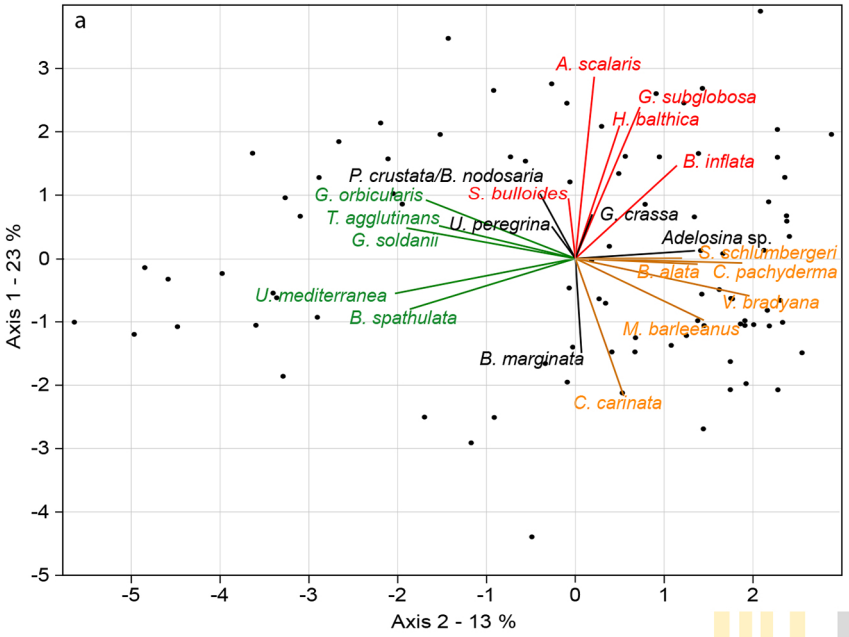

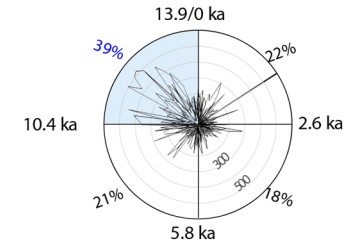

Group 1

B. spathulata : 16%, 15%, 15%, 54%
T. agglutinans : 26%, 19%, 22%, 33%
U. mediterranea : 20%, 17%, 20%, 44%
G. soldanii : 15%, 9%, 28%, 48%
G. orbicularis : 25%, 21%, 25%, 29%
V. bradyana : 27%, 26%, 19%, 29%

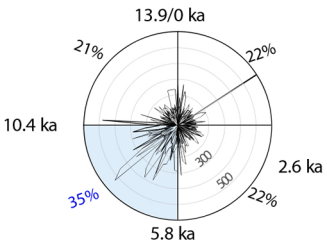

Group 2

B. in flata : 25%, 27%, 33% , 15%
A. scalaris : 20%, 20%, 32%, 28%
G. subglobosa : 20%, 20%, 43% , 17%
H. balthica : 22%, 22%, 34% , 22%
S. bulloides : 22%, 20%, 34% , 24%

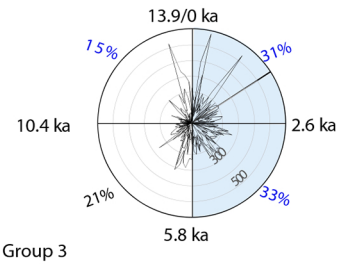

Group 3

C. pachyderma : 35%, 39% , 18%, 7%
M. barleeanus : 29%, 35% , 23%, 13%
B. alata : 28%, 30% , 28%, 14%
C. carinata : 28%, 28% , 16%, 27%
S. schlumbergeri : 34 %, 34% , 19%, 13%

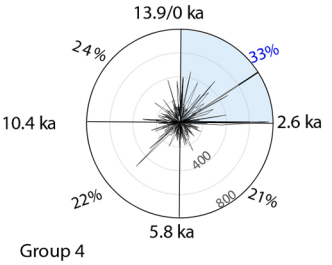

Group 4

Adelosina sp.: 31% , 20%, 23%, 26%
B. marginata : 37 %, 21%, 18%, 24%
G. crassa : 32% , 21%, 25%, 22%
U. peregrina : 33% , 23%, 22%, 22%
P. crustata B. nodosaria : 33 %, 20%, 22%, 25%

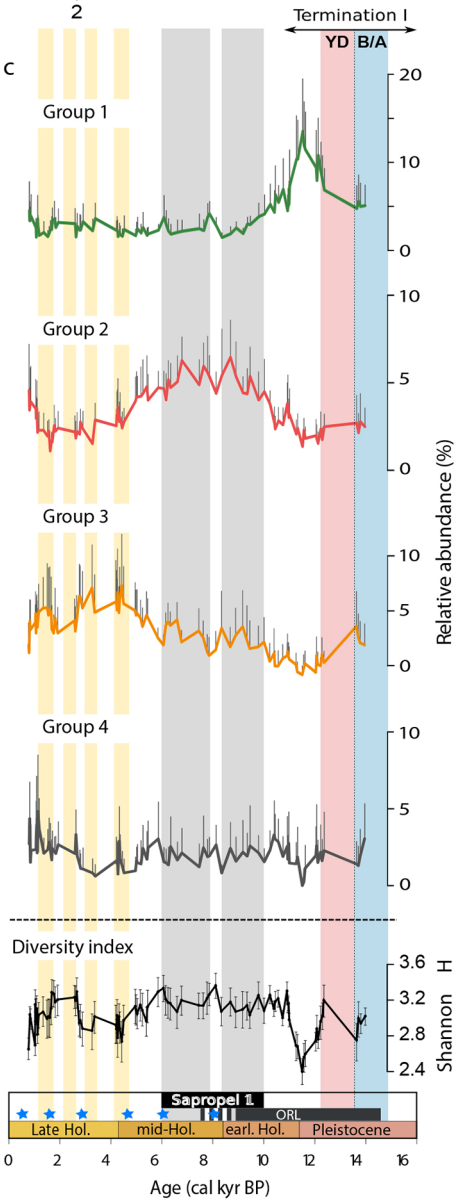

Figure 5

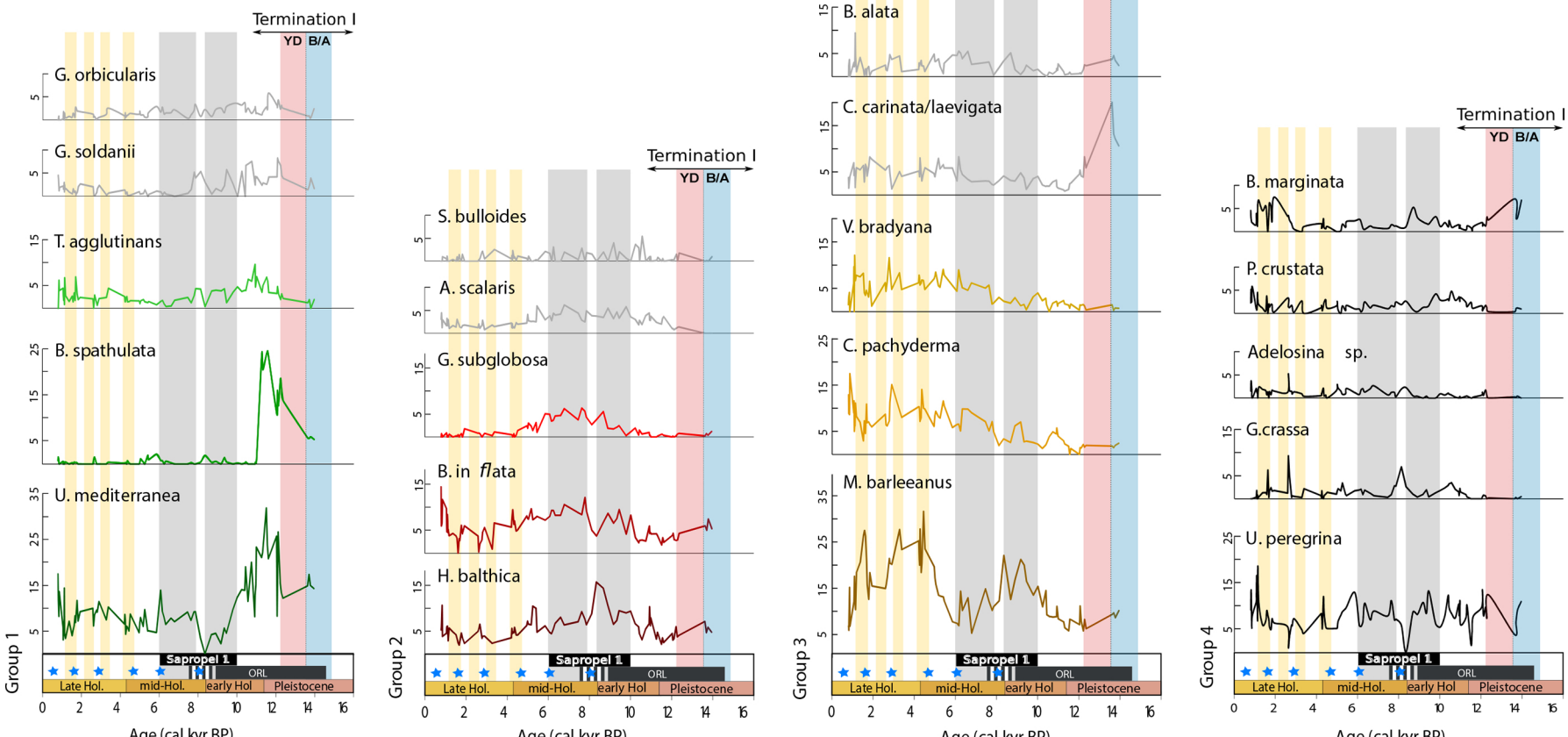
Termination I
YD B/A
G. orbicularis
G. soldanii
T. agglutinans
B. spathulata
U. mediterranea
Group 1
S. bulloides
A. scalaris
G. subglobosa
B. in flata
H. balthica
Group 2
S. schlumbergeri
B. alata
C. carinata/laevigata
V. bradyana
C. pachyderma
M. barleeanus
Group 3
B. marginata
P. crustata
Adelosina sp.
G.crassa
U. peregrina
Group 4
Sapropel 1
ORL
Late Hol.
mid-Hol.
early Hol
Pleistocene
Age (cal kyr BP)

Figure 6

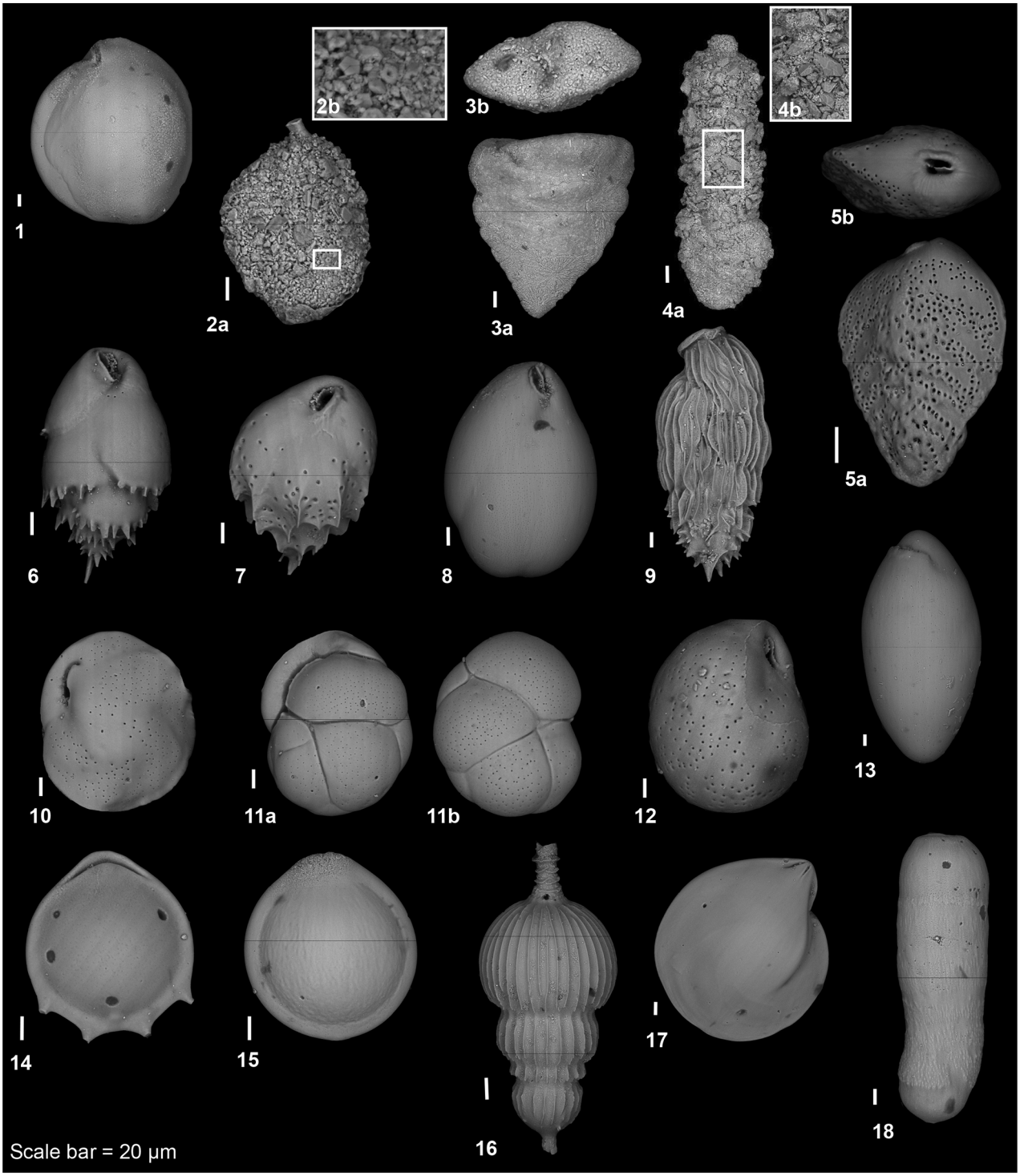

1. *Sigmoilina sigmoidea* (Brady, 1884)
2 a-b. *Sigmoilopsis schlumbergeri* (Silvestri, 1904);
2b: Magnification of the test
3 a-b. *Textularia agglutinans* d'Orbigny, 1839;
3b: Apertural view
4 a-b. *Pseudoclavulina crustata* Cushman, 1936;
4b: Magnification of the test
5 a-b. *Bolivina spathulata* (Williamson, 1858)
5b: Apertural view
6. *Bulimina marginata* d'Orbigny, 1826
7. *Bulimina inflata* Seguenza, 1862
8. *Globobulimina pacifica* Cushman, 1927
9. *Saidovina karreriana* (Brady, 1881)
10. *Cassidulina carinata (laevigata)* Silvestri, 1896
11 a-b. *Globocassidulina crassa* (d'Orbigny, 1839)
12. *Globocassidulina subglobosa* (Brady, 1881)
13. *Chilostomella oolina* Schwager, 1878
14. *Fissurina* sp.
15. *Fissurina marginata* (Montagu, 1803)
16. *Amphicoryna scalaris* (Batsch, 1791)
17. *Lenticulina convergens* (Bornemann, 1855)
18. *Siphogenerina columellaris* (Brady, 1881)

Figure 7A

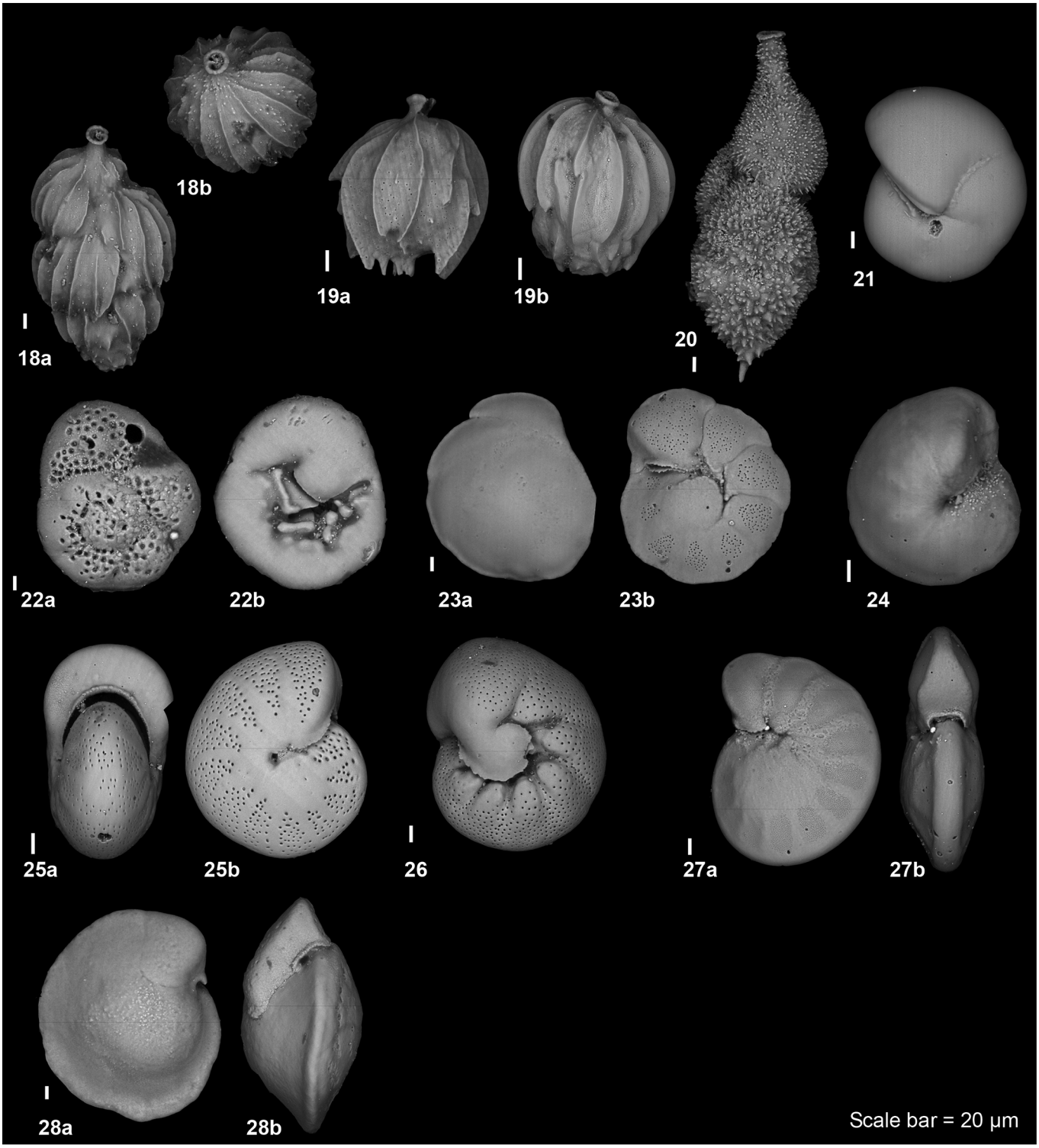

18 a-b. *Uvigerina peregrina* Cushman, 1923; 18b: apertural view
19 a-b. *Uvigerina mediterranea* Hofker, 1932
20. *Uvigerina auberiana* d'Orbigny, 1839
21. *Pullenia quinqueloba* (Reuss, 1851)
22 a-b. *Rosalina* sp.; 22a: Umbilical view; 22b: Dorsal vue
23. *Gavelinopsis praegeri* (Heron-Allen & Earland, 1913); 23a: Umbilical view; 23b: Dorsal vue
24. *Gyroidina soldanii* d'Orbigny, 1826
25 a-b. *Melonis barleeanus* (Williamson, 1858); 24a: apertural view
26. *Valvulineria bradyana* (Fornasini, 1900)
27 a-b. *Hyalinea balthica* (Schröter in Gmelin, 1791) 27a: Dorsal view; 27b: Apertural vue
28 a-b. *Cibicidoides pachyderma* (Rzehak, 1886) 28a: Umbilical view; 28b: Apertural view

Figure 7B

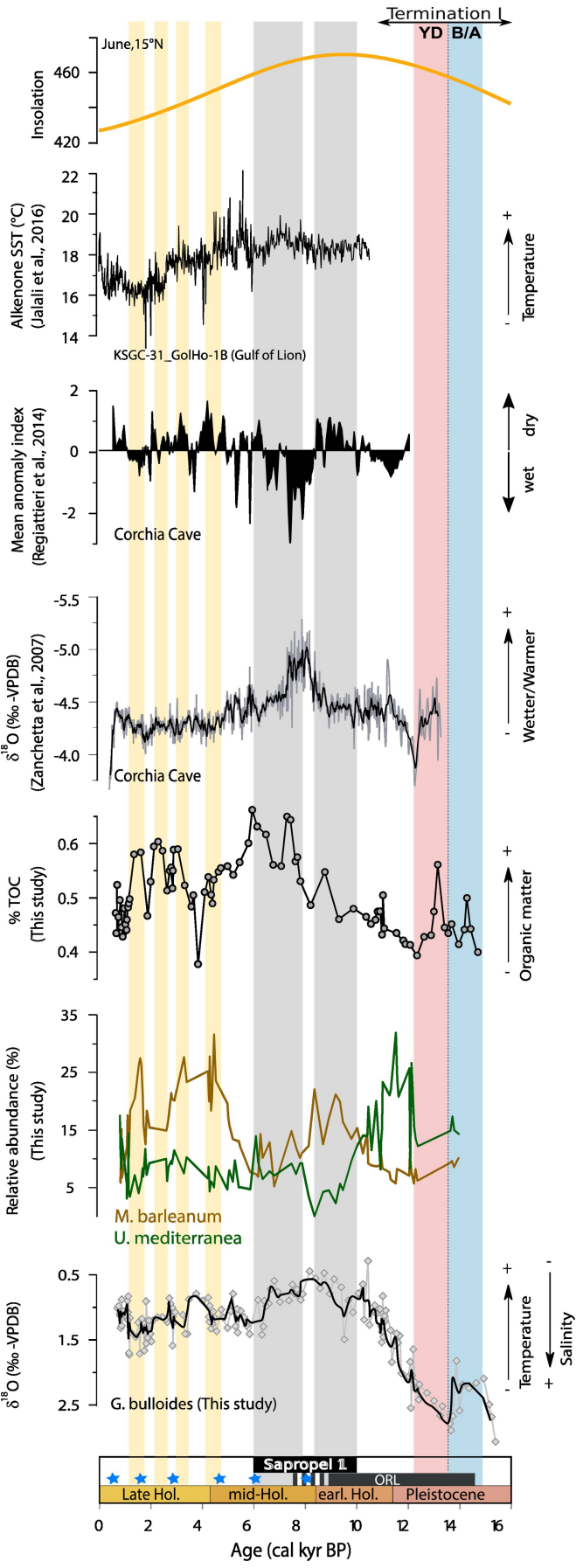
Termination I
YD
B/A
June,15°N
Insolation
460
420
Alkenone SST (°C)
(Jalali et al., 2016)
22
20
18
16
14
KSGC-31_GolHo-1B (Gulf of Lion)
+
-
Temperature
Mean anomaly index
(Regiattieri et al., 2014)
2
0
-2
Corchia Cave
wet
dry
δ18O (‰ -VPDB)
(Zanchetta et al., 2007)
-5.5
-5.0
-4.5
-4.0
Corchia Cave
Wetter/Warmer
% TOC
(This study)
0.6
0.5
0.4
Organic matter
Relative abundance (%)
(This study)
35
25
15
5
M. barleanum
U. mediterranea
δ18O (‰ -VPDB)
0.5
1.5
2.5
G. bulloides (This study)
Temperature
Salinity
Sapropel 1
ORL
Late Hol.
mid-Hol.
earl. Hol.
Pleistocene
0
2
4
6
8
10
12
14
16
Age (cal kyr BP)

Figure 8

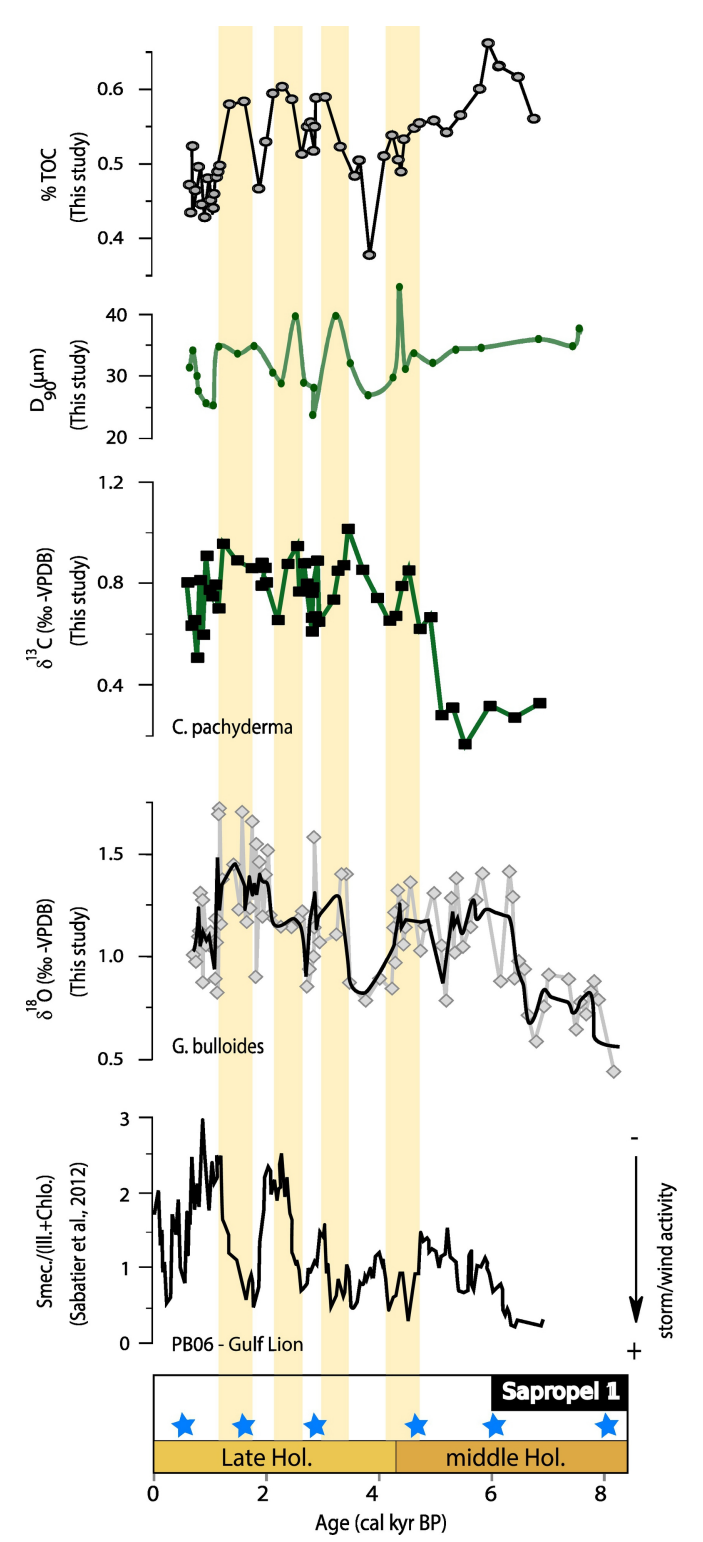
% TOC
(This study)
0.6
0.5
0.4
D90 (µm)
(This study)
40
30
20
δ13C (‰-VPDB)
(This study)
1.2
0.8
0.4
C. pachyderma
δ18O (‰-VPDB)
(This study)
1.5
1.0
0.5
G. bulloides
Smec./(Ill.+Chlo.)
(Sabatier et al., 2012)
3
2
1
0
PB06 - Gulf Lion
-
+
storm/wind activity
Sapropel 1
Late Hol.
middle Hol.
0
2
4
6
8
Age (cal kyr BP)

Figure 9

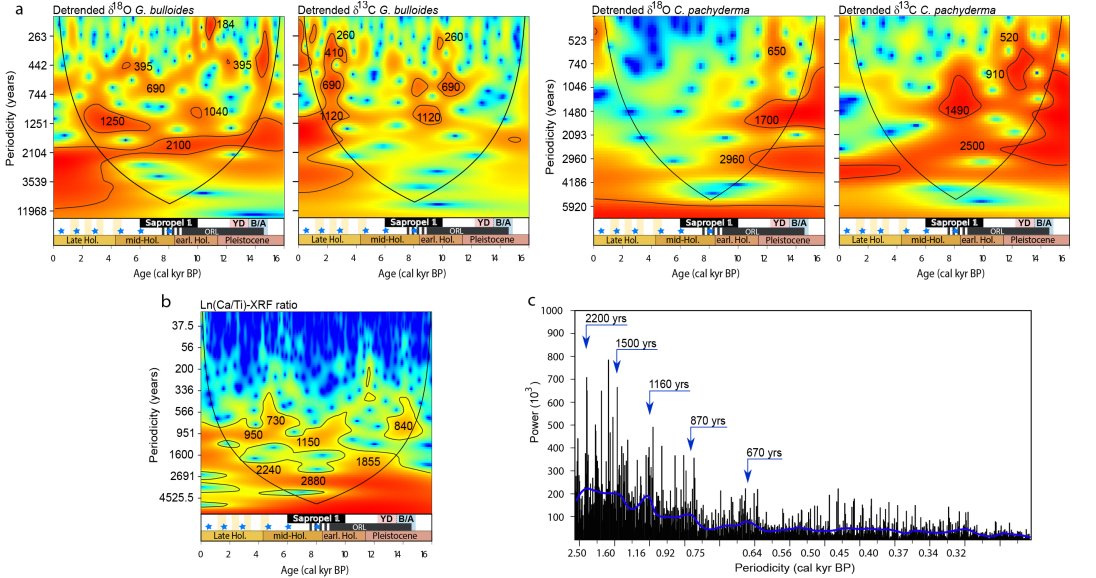
a
Detrended δ18O G. bulloides
Detrended δ13C G. bulloides
Detrended δ18O C. pachyderma
Detrended δ13C C. pachyderma
Periodicity (years)
Age (cal kyr BP)
Sapropel 1
YD
B/A
TN1
ORL
Late Hol.
mid-Hol.
earl. Hol.
Pleistocene
b
Ln(Ca/Ti)-XRF ratio
c
Power (10³)
2200 yrs
1500 yrs
1160 yrs
870 yrs
670 yrs
Periodicity (cal kyr BP)

Figure 10